Lateral septum adenosine A2A receptors control stress-induced depressive-like behaviors via signaling to the hypothalamus and habenula

Muran Wang
Wenzhou Medical University
Peijun Li
Wenzhou Medical University
Beatriz S. da Silva
University of Coimbra
Zewen Li
Wenzhou Medical University
Wu Zheng
Wenzhou Medical University
Zhenghua Xiang
Department of Neurobiology, Key Laboratory of Molecular Neurobiology of Ministry of Education and the Collaborative Innovation Center for Brain Science, Second Military Medical University
Yan He
Wenzhou Medical University
Tao Xu
State Key Laboratory of Ophthalmology, Optometry and Visual Science, Wenzhou Medical University, Wenzhou, 325027, China
Cristina Cordeiro
University of Coimbra
Lu Deng
Wenzhou Medical University
Yuwei Dai
Wenzhou Medical University
Mengqian Ye
Wenzhou Medical University
Jianhong Zhou
Wenzhou Medical University
Fenfen Ye
Wenzhou Medical University
Zhiqing Lin

Wenzhou Medical University

Xuzhao Zhou

Wenzhou Medical University

Rodrigo Cunha

University of Coimbra https://orcid.org/0000-0003-2550-6422

Jiang-Fan Chen

Wenzhou medical University

Wei Guo (guoweihaha@126.com)

Wenzhou Medical University

Article

Keywords: Depression, Lateral Septum, Adenosine A2A receptor (A2AR), Lateral habenula, Hypothalamus

Posted Date: September 14th, 2022

DOI: https://doi.org/10.21203/rs.3.rs-2007735/v1

Lateral septum adenosine A_{2A} receptors control stress-induced depressive-like behaviors via signaling to the hypothalamus and habenula

Muran Wang[1,#], Peijun Li[4,8,#], Beatriz S. da Silva[5,7], Zewen Li[1], Wu Zheng[1], Zhenghua Xiang[6], Yan He[1], Tao Xu[1], Cristina Cordeiro[5,7], Lu Deng[4,8], Yuwei Dai[1], Mengqian Ye[1], Zhiqing Lin[1], Jianhong Zhou[1], Xuzhao Zhou[1], Fenfen Ye[1], Rodrigo A. Cunha[5,9], Jiangfan Chen[2,3,*], Wei Guo[1,*]

1. The Molecular Neuropharmacology Laboratory and the Eye-Brain Research Center, The State Key Laboratory of Ophthalmology, Optometry and Vision Science, Wenzhou Medical University, Wenzhou, China

2. The Oujiang Laboratory; The Affiliated Eye Hospital, Wenzhou Medical University, 270 Xueyuan Road, Wenzhou, Zhejiang, China.;

3. The State Key Laboratory of Optometry, Ophthalmology and Vision Science, Wenzhou Medical University, Wenzhou, China.

4. Department of Neurology, The Second Affiliated Hospital and Yuying Children's Hospital of Wenzhou Medical University, Wenzhou, China

5. Faculty of Medicine, University of Coimbra, 3004-504 Coimbra, Portugal

6. Department of Neurobiology, Key Laboratory of Molecular Neurobiology, Ministry of Education, Naval Medical University, Shanghai, China

7. Portuguese National Institute of Legal Medicine and Forensic Sciences (INMLCF, IP), Coimbra, Portugal

8. Key Laboratory of Structural Malformations in Children of Zhejiang Province, Wenzhou, 325000, Zhejiang Province, China

9. CNC-Center for Neuroscience and Cell Biology, University of Coimbra, 3004-504 Coimbra, Portugal

[#] These authors have contributed equally to this work and share first authorship

*** Correspondence:**

Wei Guo

guoweihaha@126.com

Jiang-fan Chen

chenjf555@gmail.com

Conflict of interest: The authors have declared that no conflict of interest exists.

Abstract

Depression is the single largest contributor to the burden of disease, yet the current antidepressant medications are limited by high non-responsiveness and significant side effects. The lateral septum (LS) is thought to control of depression, however, the cellular and circuit substrates are largely unknown. Here, we identified a subpopulation of LS GABAergic adenosine A_{2A} receptors ($A_{2A}R$)-positive neurons mediating depression via direct projects to the lateral habenula (LHb) and the hypothalamus. Activation of $A_{2A}R$ in the LS augmented the spiking frequency of $A_{2A}R$-positive neurons leading to a decreased activation of surrounding neurons. Accordingly, modulation of LS-$A_{2A}R$-positive neurons activity via optogenetic stimulation formatted depressive-like phenotype and the optogenetic activation of LS-$A_{2A}R$-positive neurons projection terminals to the LHb or the hypothalamus, phenocopied depressive behaviors. Moreover, we shown a selective upregulation of $A_{2A}R$ in the LS in two mouse models of repeated stress-induced depression and in postmortem brains of suicide completers suffered from depression disorder, and the bi-directional manipulation of LS-$A_{2A}R$ activity demonstrated that LS-$A_{2A}R$s are necessary and sufficient to trigger depressive phenotypes. This identification that aberrantly increased $A_{2A}R$ signaling in the LS is a critical upstream regulator of repeated stress-induced depressive-like behaviors provides a neurophysiological and circuit-based justification of the antidepressant potential of $A_{2A}R$ antagonists, prompting their clinical translation.

Keywords: Depression, Lateral Septum, Adenosine A_{2A} receptor ($A_{2A}R$), Lateral habenula, Hypothalamus

Introduction

Depression is the single largest contributor to the burden of disease, affecting more than 300 million people worldwide (1). A major risk of depression is suicide ideation, with over 65% of suicide completers being affected by mood disorders (2). The traditional antidepressant treatments, such as with selective serotonin reuptake inhibitors, are limited by slow onset of therapeutic effects, limited effect size and high proportions of non-responsive patients and the newly emerging fast-acting antidepressant, such as ketamine, are associated with significant side effects such as addiction propensity (3). Thus, the identification of novel and effective therapeutic targets to develop antidepressants is critically needed.

The lateral septum (LS), a midline brain structure, has been implicated in a wide variety of functions, such as emotional, motivational, and social behavior (4, 5). Evidence is accumulating to relate an abnormal function of the LS with a directional control of stress-induced depressive behavior (reviewed in (4, 6)): from alterations in neural activity within the LS that correlate with the development of behavioral manifestations of depression in animal models, to the effects of antidepressant drugs on LS functioning, to antidepressant-like effects of cell signaling processes in LS neurons. Recent studies have identified that LS-GABAergic neurons trigger depression-related behaviors through their periaqueductal gray projections (7), while somatostatin-positive neurons in LS also influence depression-like behaviors (8). However, disentangling the precise LS circuitry associated with depressive phenotypes is still far from clear, since the LS is constituted by a majority of GABAergic neurons forming multiple superimposable circuits inter-linked by intra-septal intrinsic sub-circuits, so that LS sub-circuits often antagonize each other to influence behavioral outputs (4, 9). The problem is, in part, due to the complex architecture based on selective gene expression, especially the neuromodulatory receptors (9). Recently, we have found the expression of adenosine A_{2A} receptors ($A_{2A}R$), an important neuromodulatory receptor (10, 11), in LS via a novel knock-in transgenic mouse line (12), which raise our interesting to explore its role in the regulation of depression.

93 Convergent epidemiological, genetic and pharmacological findings support a role of $A_{2A}R$ as a novel
94 therapeutic target for depression. Human epidemiological investigation into dietary factors associated
95 with depression unveiled that the consumption of caffeine, the most widely consumed psychoactive
96 drug, by acting as a non-selective adenosine receptor antagonist (13, 14), is inversely correlated with
97 depression and the likelihood of suicide in several cohorts (reviewed in (15, 16)). Also, polymorphisms
98 of the human $A_{2A}R$ gene are associated with the incidence and clinical heterogeneity of depression
99 (17). This potential link of adenosine signaling with depression is attractive since depression is
100 intrinsically linked to chronic stress, adenosine levels are increased upon brain stressful conditions
101 (reviewed in (18)) and the upregulation of $A_{2A}R$ in different brain regions is a proposed biomarker of
102 the onset of neuropsychiatric diseases (19). The stress-induced alterations of the adenosine
103 neuromodulation system are initially homeostatic in nature, but their persistent alteration upon
104 chronic stress results in synaptic dysfunction (18), which has been proposed to underlie depressive-
105 like behaviors (20). Indeed, repeated restraint stress (21) and chronic unpredictable stress (22) induce
106 the upregulation of synaptic $A_{2A}R$ and the genetic deletion or pharmacological blockade of $A_{2A}R$
107 attenuate maladaptive features in various depressive-like behavioral paradigms (21-26). Notably, the
108 antidepressant-like effect size of $A_{2A}R$ antagonists is equivalent to that of classical antidepressants
109 such as desipramine in the rat learned helplessness model (25). Although the use of forebrain $A_{2A}R$
110 knockout mice has pinpointed a role for central $A_{2A}R$ in the control of depressive-like phenotypes (22),
111 $A_{2A}R$ are located in different types of neurons in different limbic cortical areas that are associated with
112 depression (27), including ventral tegmental area (VTA), medial prefrontal cortex (mPFC), lateral
113 habenula (LHb), LS, amygdala and hippocampus. So, to identify the critical locus and neural circuits for
114 $A_{2A}R$ antagonism to elicit antidepressant activity is still a key hurdle for the acceptance and
115 development of $A_{2A}R$-based therapies.

116 In the present study, we have identified a subpopulation of LS GABAergic $A_{2A}R$-positive neurons
117 mediating depression via direct projects to the LHb or the hypothalamus. Furthermore, the selective
118 increased $A_{2A}R$ activity in the LS, shown in two chronic stress-induced depression mice models, was

119 necessary and sufficient for development of depressive-like behaviors. Consistently, an upregulation
120 of $A_{2A}R$ was found in the LS of suicide completers suffered from depression disorder. Given the noted
121 clinical safety profile of $A_{2A}R$ antagonists (28), these new insights offer a novel opportunity to treat
122 depressive disorders by targeting LS-$A_{2A}R$ signaling.

Results

1. $A_{2A}R$ Expression Identifies a Subset of GABAergic LS Neurons

In our previous study, $A_{2A}R$ were observed in the LS and no staining was detected in the medial septum or the horizontal and vertical limbs of the diagonal band. To identify the projection areas of LS-$A_{2A}R^+$ neurons, AAV2/9-syn-DIO-EYFP were injected into the LS of $A_{2A}R$-Cre mice. Three weeks after injecting, the EYFP-positive projection terminals (*i.e.* from LS-$A_{2A}R^+$ neurons) were found to target the dorsomedial hypothalamus (DMH) and the lateral habenula (LHb) (Figure 1A). To further validate the direct connection between LS and DMH or LHb, we used an AAV-mediated anterograde trans-synaptic tagging system (29). An AAV2/1-hsyn-mcherry-cre virus was injected into the LS, and AAV2/9-syn-DIO-EYFP virus was injected into the DMH or LHb. Three weeks later, fluorescence imaging confirmed the direct projections from the LS to the LHb and DMH (Figure 1B) .

To explore the cellular effect of the $A_{2A}R$ signaling in the LS, we determined the effect of the $A_{2A}R$ agonist CGS21680 on neuronal firing of LS-$A_{2A}R^+$ neurons by *in vitro* electrophysiological recordings in acute brain slices from adult $A_{2A}R$-Cre mice injected with AAV2/9-syn-DIO-EYFP into the LS. The activity of EYFP-positive cells (*i.e.* LS-$A_{2A}R^+$ neurons) was recorded using a cell-attached voltage-clamp mode in low-Mg^{2+} (1 mM) aCSF solution with biocytin (1%, Thermo Scientific) in the intracellular solution. This allowed a *post-hoc* morphological characterization of the recorded EYFP-positive neurons, which showed that $A_{2A}R^+$ neurons possessed long and numerous branches (Figure 2A). A subsequent immunofluorescent staining of slices revealed that LS-$A_{2A}R^+$ neurons were GABAergic rather than glutamatergic neurons (Figure 2B). Moreover, single cell RT-PCR analysis of the total mRNA isolated from recorded cells also confirmed that all recorded EYFP-positive cells were GABAergic neurons (Figure 2C). Activation of $A_{2A}R$ by CGS21680 (30 nM) significantly increased the firing frequency of EYFP-positive neurons (Figure 2D), indicating that $A_{2A}R$ activation augments neuronal activity of LS-$A_{2A}R^+$ neurons. The effect of CGS21680 was reversible after washout (Figure 2E).

Previous investigations have demonstrated that the systemic or local administration of diverse antidepressants increases the neuronal firing rate of the LS, whereas some stressful situations decrease its firing rate (6). To determine the effects of $A_{2A}R$ on the LS circuitry, we first determined the effect of CGS21680 on non-$A_{2A}R^+$ neurons in LS by *in vitro* electrophysiological recordings in brain slices of $A_{2A}R$-Cre mice injected with AAV-syn-DIO-EYFP. We found that $A_{2A}R$ activation by CGS21680 (30 nM) reduced the frequency (but not amplitude) of spontaneous inhibitory postsynaptic currents (sIPSCs) of neurons around EYFP-positive cells, which likely resulted from the increase of $A_{2A}R^+$ GABAergic inputs to non-$A_{2A}R$ positive neurons in the LS (Figure 2F).

To next determine the effects of $A_{2A}R$ on the activity of the LS as a whole, we measured c-Fos expression in the LS after the focal infusion in the LS of either CGS21680 (5 μg/μL, 2 μL per injection) or vehicle (Figure 3A). The focal microinjection of CGS21680 into the LS decreased the number of c-Fos-positive neurons in the LS compared to vehicle-treated mice (Figure 3B). Furthermore, we found that CGS21680 infusion into the LS induced a robust upregulation of c-Fos expression in the LHb and DMH compared to PBS-treated mice (Figure 3C).

2. Optogenetic modulation of the activity of LS-$A_{2A}R^+$ neurons formats depressive-like phenotype

As the LHb and DMH are important regions involved in depression regulation (30) (31), we next investigated the selective role of LS-$A_{2A}R^+$ neurons in the regulation of depressive behavior. We injected the AAV2/9-hEF1a-DIO-ChR2-EYFP or its control virus AAV2/9-hEF1a-DIO-EYFP (200 nL) into the LS of $A_{2A}R$-Cre mice and implanted the optical fibers in the LS (Figure 4A). Three weeks after viral expression, optogenetic activation of LS-$A_{2A}R^+$ neurons increased the immobility time in the TST compared to the control virus group (Figure 4B), without affecting either the total travelled distance and the time spent in the center area in the OFT (Figure 4C, D) or the time spent in the open arms in the O maze (Figure 4E). Thus, the optogenetic activation of LS-$A_{2A}R^+$ neurons induced some traits of a depressive-like phenotype. Furthermore, selective inhibition of corresponding circuit elements

showed opposing behavioral effects compared with excitation. We injected the AAV2/9-hEF1a-DIO-eNpHR3.0-EYFP or its control virus AAV2/9-hEF1a-DIO-EYFP (200 nL) into the LS of A_{2A}R-Cre mice and implanted the optical fibers in the LS (Figure 4F). Three weeks after viral expression, optogenetic inhibition of LS-$A_{2A}R^+$ neurons decreased the immobility time in the TST compared to the control virus group (Figure 3G) and did not modify behavior in both OFT and O-maze test (Figure 4H-J).

3. Optogenetic activation of the LS^{A2AR+}→DMH and LS^{A2AR+}→LHb projections reproduced the induction of depressive-like behaviors

The identification of the functional connectivity of the LS^{A2AR+}→DMH and LS^{A2AR+}→LHb, together with the important role of the hypothalamus and habenula in the control of mood behaviors, led us to investigate a putative critical role of LS→LHb projections and LS→DMH projections in the induction of depressive-like behaviors. We achieved the targeted expression of ChR2 in $A_{2A}R^+$ projection terminals by injecting the AAV2/9-hEF1a-DIO-ChR2-EYFP or its control virus AAV2/9-hEF1a-DIO-EYFP (200 nL) into the LS of A_{2A}R-Cre transgenic mice. We implanted the optical fibers in the DMH or LHb (Figure 5A, E). Optogenetic activation of the LS^{A2AR+}→DMH projections increased the immobility time in the TST compared to the control virus group (Figure 5B). There was no difference in the total travelled distance or in the time spent in the central area in the OFT between the ChR2 group and the control group (Figure 5C, D). Similarly, optogenetic activation of the LS^{A2AR+}→LHb projections increased the immobility time in the TST (Figure 5F), without affecting the total distance travelled or the time spent in the central area of the OFT (Figure 5G, H). Thus, optogenetic activation of the projection terminals from the LS-$A_{2A}R^+$ neurons to the DMH and LHb reproduced the induction of depressive-like behaviors. Together with the viral tracing results, these findings established that the LS^{A2AR+}→DMH and the LS^{A2AR+}→LHb pathways mediate the depressive-like behavior caused by abnormally elevated A_{2A}R activity in LS.

4. $A_{2A}R$ are upregulated selectively in the LS in two mouse models of chronic stress

Since the upregulation of $A_{2A}R$ is a proposed biomarker of the dysfunctional brain circuits at the onset of brain diseases (19), whether $A_{2A}R$ is an inducible factor under stress conditions is an interesting question. We determined alterations of $A_{2A}R$ density in multiple brain regions associated with mood processing in two chronic stress models. First, after chronic restraint stress (CRS) exposure for 14 days, CRS-mice showed an increase in immobility time in the tail suspension test (TST), without change of locomotion in the open field test (OFT), and of the time spent in the open arms in the elevated O-maze test (Figure 6A-D). After behavioral testing, mice were immediately sacrificed and $A_{2A}R$ immunodensity was probed in several mood-associated brain regions, including septum, prefrontal cortex (PFC), hippocampus, and striatum (Figure 6E, F). Compared to the control group, mice subjected to CRS displayed a selective upregulation (2.06 times of control, $P<0.001$) of $A_{2A}R$ in the septum. Although $A_{2A}R$ immunodensity varied considerably across samples, we observed a trend for $A_{2A}R$ up-regulation also in PFC and hippocampus, whereas the levels of $A_{2A}R$ remained unchanged in striatum, consisting with previous Western blotting analyses (32, 33).

We also evaluated the regional pattern of $A_{2A}R$ upregulation in a second stress paradigm, the 5-day repeated forced swim stress paradigm, described in a previous study (34). Compared to control mice, stressed mice showed an increased immobility time in the forced swimming test (FST), without changes in the total distance of movement in the OFT (Figure 7A, B). 5d-RFSS-mice spent less time in the center area of OFT but similar time in the open arms of an elevated O-maze test compared to the control group (Figure 7C, D), consistent with previous reports [29]. After behavioral testing, the analysis of $A_{2A}R$ levels in the septum, PFC, hippocampus, striatum and hypothalamus revealed a selective increase (4.36 times of control, $P<0.01$) of $A_{2A}R$ density in the septum without significant changes in the 3 other brain regions (Figure 7E, F), as previously observed in the CRS model.

5. $A_{2A}R$ overexpression in the LS is sufficient to induce a depression-like phenotype

We next investigated whether the $A_{2A}R$ overexpression in the LS was sufficient to trigger a depressive-like behavior. We confirmed achieving an $A_{2A}R$ overexpression in the LS by bilateral injections of $A_{2A}R$-expressing virus (AAV2/9-hSyn-$A_{2A}R$-3xflag-ZsGreen) but not control virus (AAV2/9-hSyn-ZsGreen) (Figure 8A, B). Three weeks after the viral injection, behavioral analysis revealed that mice transfected with $A_{2A}R$-expressing virus displayed increased immobility in the TST (Figure 8C). There was no difference in the total travelled distance and in the time spent in the center area in the OFT (Figure 8D, E) nor in the time spent in the open arms in the O maze (Figure 4F), between mice injected with the $A_{2A}R$-expressing virus and with the control virus. Furthermore, LS-$A_{2A}R$ overexpression also decreased the consumption of sucrose compared with the control group (Figure 8H) and showed no difference in the total consumption of liquid (Figure 8G). Thus, $A_{2A}R$ overexpression in the LS was sufficient to induce despair-like behavior, indicating that $A_{2A}R$ upregulation is a trigger rather than only a biological marker of depressive-like behavior.

6. Focal genetic and pharmacological $A_{2A}R$ inactivation selectively in the LS attenuate depressive-like phenotype

To further test the function of endogenous $A_{2A}R$ activity *in vivo*, we determined the effect of shRNA knockdown of LS-$A_{2A}R$ on depressive-like behaviors. We achieved focal knockdown of LS-$A_{2A}R$ by injection into the LS of AAV2/9-syn-$A_{2A}R$shRNA-GFP ($A_{2A}R$-shRNA) or control virus (AAV2/9-syn-$A_{2A}R$shcontrol-GFP, ctrl-shRNA) (Figure 9A). Focal knockdown of LS-$A_{2A}R$ reduced immobility in TST (Figure 9B) without affecting spontaneous motor activity and the time spent in the central area in the OFT (Figure 9C, D). Furthermore, LS-$A_{2A}R$ knockdown also increased the consumption of sucrose compared with the control group (Figure 9F) and showed no difference in the total consumption of liquid (Figure 9E). Thus, the selective knockdown of $A_{2A}R$ in the LS produced antidepressant-like behaviors.

To explore the translational potential of pharmacological targeting LS-$A_{2A}R$, we determined the ability of the locally applied $A_{2A}R$ antagonist KW6002 (recently approved anti-parkinsonian by US-FDA (28)) to reverse the chronic stress-induced depressive phenotypes (Figure 9G). Mice were first exposed to either CRS or no-stress stimuli for 14 consecutive days. CRS mice with a confirmed depressive-like phenotype (Figure 9H-J) or no-stress mice were randomly assigned for treatment of KW6002 (by unilateral intra-LS infusion of KW6002, 0.5 µg/µL, 2 µL per injection) or vehicle (methylcellulose) daily for three consecutive days. As expected, CRS-mice treated with vehicle displayed depressive-like behavior as indicated by increased immobility in the TST. LS infusion of KW6002 not only decreased the immobility time in the non-stress mice, but also reversed the increased immobility time induced by CRS, without affecting either locomotion or the time spent in the center in the OFT (Figure 9K-M). Importantly, two-way ANOVA analysis indicated that there was a CRS x KW6002 treatment interaction (p=0.0436), indicating that KW6002 preferentially reverted the CRS-induced depressive-like behavior. Thus, pharmacological blockade of LS-$A_{2A}R$ can reverse the depressive-like phenotype caused by CRS.

7. $A_{2A}R$ are upregulated in the postmortem LS of suicide completers

To confirm the clinical relevance of LS-$A_{2A}R$ upregulation upon depression, we analyzed alterations of $A_{2A}R$ density in the dissected LS from postmortem samples collected from suicide completers, since over 65% of suicide completers are affected by mood disorders (2). We carried out a receptor binding quantification using a selective but supramaximal concentration of 2 nM of the $A_{2A}R$ antagonist [^{3}H]SCH58261. This was inferred from the saturation isotherm of [^{3}H]SCH58261 binding to membranes of the subgenual area BA25 of 5 controls aged between 42 and 61 years (3 men and 2 women), which revealed a K_D of 0.83 nM (95% confidence interval of 0.68-0.98 nM) and a B_{max} of 23.6±1.6 fmol/mg protein (Figure 10A). Thus, after quality control validation (see Methods), LS samples from 6 males and females suicide completers and 5 age-matched subjects of both sexes, death from natural causes or road accidents, were processed to obtain total membranes as well as synaptosomal membranes.

We report that $A_{2A}R$ binding density in the synaptosomal membranes of the LS increased two-fold in suicide completers compared to control subjects (Figure 10B; $P<0.05$). This increase of $A_{2A}R$ binding density was selective for synaptosomal membranes since the $A_{2A}R$ binding in total membranes of the LS was not different between the suicide completers and controls (Figure 10B; $P=0.0519$). This finding provides the first clinical evidence for $A_{2A}R$ upregulation in the LS upon putative mood dysfunction.

Discussion

The present study allowed identifying the LS $A_{2A}R$-positive neurons as direct upstream integrative regulators of depressive-like behavior, as supported by four convergent sets of experimental findings: (i) the upregulation of $A_{2A}R$ in the LS in two chronic stress mouse models and in suicide completers; (ii) the sufficiency and necessity of $A_{2A}R$ activation in the LS to produce depressive-like behaviors; (iii) $A_{2A}R$ activation in LS-$A_{2A}R^+$ neurons increased their neuronal firing leading to a suppressed activity of their surrounding LS neurons; (iv) the emergence of depressive-like behavior upon activation of LS-$A_{2A}R^+$ neurons by signaling via their downstream LS-$A_{2A}R^+$→LHb and LS-$A_{2A}R^+$→DMH pathways. This cellular and neural circuit dissection prompts a rationale to understand the antidepressant effects of $A_{2A}R$ antagonists, based on a novel working model whereby aberrantly enhanced LS-$A_{2A}R$ signaling mimics stressor signals to trigger depressant behavior: LS-$A_{2A}R^+$ GABAergic neurons sense information from internal and external stressors upregulating $A_{2A}R$ signaling to increase their firing rate and to simultaneously decrease LS activity and activate the LS-$A_{2A}R^+$→LHb and LS-$A_{2A}R^+$→DMH pathways to trigger depressant-like behaviors.

These findings align with the involvement of LS circuitry in the expression of chronic stress-induced depressive like behavior. Amongst this complexity of LS circuitry, we teased apart the functional relevance of LS-$A_{2A}R^+$ neurons that emerged as key orchestrators of stress-induced depressive-like behavior. LS-$A_{2A}R^+$ neurons were essentially GABAergic neurons and the pharmacological activation of $A_{2A}R$ increased their firing frequency. This coincides with the ability of $A_{2A}R$ to bolster the activity of defined populations of GABAergic neurons in other brain structures such as in the hippocampus (35), central amygdala (36), prefrontal cortex (37), globus pallidus (38), tuberomammillary nucleus (39) or in the nucleus of the solitary tract (40). The activation of LS-$A_{2A}R^+$ GABAergic neurons lead to a suppression of the activity of surrounding LS cells, as concluded by a decreased c-Fos-immunoreactivity. This is in agreement with the general conclusion that the LS acts a mood regulator

304 exerting a tonic inhibition onto various subcortical nuclei (reviewed in [24,28]), as heralded by the
305 evidence that activation of LS neurons endowed with dopamine D3 receptors rescues early life stress-
306 induced social impairments (41), the metabotropic Glu2/3 receptor agonist LY379268-induced
307 increase of LS activity relieves stress-induced social withdrawal symptoms (42), activation of Takeda
308 G protein-coupled receptor 5 increases somatostatin-GABAergic neurons of the dorsolateral septum
309 decreasing depressive-like symptoms (8), genetic elimination of neuroligin-2 reduces LS inhibition to
310 stress-induced activation of downstream hypothalamic nuclei reducing avoidance behavior (43) and a
311 $5HT_{1A}$ receptor agonist increases LS activity to suppress the HPA axis and increase escape behavior in
312 a forced swimming stress model (37).

313

314 In the present study, we characterized the specific downstream targets of the LS-$A_{2A}R^+$ neurons
315 involved in the control of stress-induced mood dysfunction, since distinct LS neuron populations
316 project to different downstream targets to exert distinct behavioral modulation (reviewed in (4)). Our
317 circuit level analysis identified the LS-$A_{2A}R^+$→ dorsomedial hypothalamus (DMH) and LS-$A_{2A}R^+$→lateral
318 habenula (LHb) pathways as the main downstream target for top-down control of depressive-like
319 behavior by LS-$A_{2A}R$. The DMH is a main established output of the LS, establishing a feedback loop to
320 control LS circuits through peptidergic signals such as CRF and vasopressin, which is proposed to be
321 involved in depression, fear and anxiety (reviewed in (4, 6)). In agreement with this important role of
322 the DMH, our virus tracing using $A_{2A}R$-Cre mice identified the DMH as the main downstream target of
323 LS-$A_{2A}R^+$ neurons through a direct projection. Furthermore, activation of LS-$A_{2A}R^+$ neurons produced a
324 more robust increase of c-Fos in the DMH. Critically, optogenetic activation of the LS-$A_{2A}R^+$→DMH
325 pathway recaptured the depressant phenotype of LS-$A_{2A}R$ activation. Based on the parallel effects of
326 $5HT_{1A}$ receptor agonists and of $A_{2A}R$ antagonists (25, 44) and the proposed heteromerization of both
327 receptors (45), the previously identified bidirectional ability of LS-$5HT_{1A}$ receptors to control the HPA
328 axis and define stress-induced mood alterations (37), prompts the proposal that LS-$A_{2A}R$ may also
329 control CRH release and HPA axis in the DMH. This contention provides a tentative mechanism for the

recent finding that $A_{2A}R$ blockade reverts the depressive-like behavioral, electrophysiological and morphological alterations induced by early-life maternal separation through a restoration of the activity of the HPA axis (33).

Our circuit level analysis also identified the involvement of an unreported LS-$A_{2A}R^{+}$⟶LHb pathway in the stress-induced expression of depressive-like behavior. This conclusion was based on the combined observations that: (i) virus tracing identified the LHb as a downstream target of LA-$A_{2A}R^{+}$ neurons; (ii) c-Fos expression analysis confirmed the functional activation of LS-$A_{2A}R$-LHb pathway upon LS-$A_{2A}R$ activation, in accordance with a recently identified stress-induced functional circuit from LS to LHb (46); (iii) optogenetic activation of LS-$A_{2A}R^{+}$→LHb projections induced depressant effects. The identification of the LS-$A_{2A}R^{+}$→LHb pathway as a downstream target for LS-$A_{2A}R$ control of depressive-like behavior is consistent with the role of the LHb in the development of depression, as heralded by the persistent and robust activity in the LHb of depressed animals (47, 48) (reviewed in (49)), by the experimental ability of increased LHb activity to trigger depressive-like behaviors (50-52), by the ability of the fast-acting antidepressant drug ketamine to wane LHb neuronal activity (53) and by the impact of deep-brain stimulation in the LHb to alleviate depressive-like symptoms (54, 55). While the specific types of neurons in the LHb controlled by the LS-$A_{2A}R^{+}$ neurons still await to be identified, LS-$A_{2A}R$ signaling is concluded to be an upstream regulator of the LHb to implement stress-induced depressive-like maladaptive behavior.

While previous studies have demonstrated that systemic administration of $A_{2A}R$ antagonists or genetic inactivation of $A_{2A}R$ produces antidepressant effects, the critical action site for $A_{2A}R$ to control depressive-like behavior was unclear. $A_{2A}R$ are enriched in the striatum with a predominant post-synaptic localization to control dopamine signaling (56), with comparatively lower densities in brain regions associated with depression, such as mPFC, hippocampus and amygdala (57, 58), where $A_{2A}R$

are mostly presynaptic controlling synaptic plasticity (reviewed in (18)) and synaptic remodeling (59). Altered functioning of neuronal networks leads to a maladaptive up-regulation of $A_{2A}R$, which constitutes a biomarker of progressive synaptic failure and neurodegeneration (19). This has been documented in hippocampal synapses in models of Alzheimer's disease (60), in cerebrocortical synapses in models of epilepsy (61, 62) or of Rasmunsen encephalopathy (63), in corticostriatal synapses in models of Huntington's disease (64) or of restless leg syndrome (65) or in cerebellar synapses in models of spinocerebellar ataxia (66). We now identified a stress-induced aberrant up-regulation of $A_{2A}R$ in the LS, which occurred selectively in synapses in the LS of suicide completers and was more robust compared with the prefrontal cortex, hippocampus and striatum in two chronic stress models. Overall, these findings prompt LS-$A_{2A}R$ as a central adaptive feature relating stress exposure and $A_{2A}R$-mediated modulation of chronic stress-induced depressive-like behavior.

In summary, we have uncovered and identified aberrantly increased $A_{2A}R$ signaling in the LS as a key upstream regulator for stress-induced depressive-like behavior by controlling LS activity and signaling through the LS-$A_{2A}R^{+}$→DMH and LS-$A_{2A}R^{+}$→LHb pathways. This new understanding of the precise circuit targets of LS-$A_{2A}R$ signal as an upstream and integrated regulator of stress-induced depressive-like behavior provides the required rationale to expand the clinical translation of $A_{2A}R$ antagonist as a potentially novel and effective anti-depressant, which has already been recently approved by US-FDA for the treatment of Parkinson's disease with a notable safety profile (28).

Materials and methods

Animals

Male adult C57BL/6J mice (8-16 weeks of age, Shanghai JieSiJie Laboratory Animal Co., Ltd.) and male $A_{2A}R$-Cre mice (8-16 weeks of age, MMRRC, Stock Number: 031168-UCD) were maintained and used

in accordance with protocols approved by the Institutional Ethics Committee for Animal Use in Research and Education at Wenzhou Medical University, China. Mice were housed 3-5 per cage in a suitable temperature (23 ± 1 °C) and relative humidity room (60 ± 2%) under a 12 h light/ dark cycle (light on from 8 a.m. to 8 p.m.) with *ad libitum* food and water, unless otherwise specified.

Viral Vectors

AAV2/9-hsyn-hA_{2A}R-3fxflag-ZsGreen (titre: 1.5E+12 vector genome (v.g.)/mL, Hanbio Biotechnology), AAV2/9-hSyn-ZsGreen (titre: 1.8E+12 v.g./mL, Hanbio Biotechnology), AAV2/9-A_{2A}R-shRNA-GFP (titre: 1.5E+12 v.g./mL, Taitol Biotechnology), AAV2/9-A_{2A}R-shcontrol-GFP (titre: 1.5E+12 v.g./mL, Taitol Biotechnology), rAAV2/9-Ef1a-DIO-hChR_2(H134R)-EYFP (titre: 2.0E+12 v.g./mL, BrainVTA), AAV2/9-hEF1a-DIO-eNpHR3.0-EYFP(titre: 5.94E+12 v.g./mL, BrainVTA), rAAV2/9-EF1a-DIO-EYFP (titre: 2.0E+12 v.g./mL, BrainVTA), rAAV2/9-hsyn-DIO-EYFP (titre: 5.14E+12 v.g./mL, BrainVTA), AAV2/1-hSyn-mcherry-A_{2A}R-Cre (titre: 1.19E+13 v.g./mL, OBiO Technology), AAV2/9-syn-EGFP (titre: 1.2E+12 v.g./mL, Hanbio Biotechnology).

Stereotaxic Surgery, AAVs microinjection and Optical Fiber Implantation

For stereotaxic surgery, animals were anesthetized with Avertin (250 mg/kg, Sigma-Aldrich). Virus were ipsilateral or bilaterally injected by a pressure microinjector with a pulled glass capillary into the different brain regions according to the different experiments: LS (+0.8 mm AP; ±0.35 mm ML; -2.75 mm DV from the brain surface), LHb (-1.72 mm AP; ±0.46 mm ML; -2.7 mm DV), DMH (-1.70 mm AP; ±0.5 mm ML; -5.0 mm DV). Volumes of virus ranged between 100-200 nL (at the rate of 20 nL/min) per side. The capillary was left in the brain for 5-10 min after the injection. Mice were put on a heat pad for recovering from anesthesia after the surgery. The viral injection sites were verified by post immunohistochemistry experiment.

For optic fiber implantation, 200 μm diameter optic fibers (Newdoon Technology) were implanted 0.05 mm above the virus injection site and fixed to the skull using dental cement.

Cannula Infusion Experiment

The cannula (customized by Kedou (Suzhou) Brain-computer Technology Co., Ltd), constituted by a hollow catheter (0.5 mm outer diameter) and a protective cap containing the inner core (outer diameter is 0.25 mm), was ipsilateral implanted into the LS of C57BL/6J mice. After the surgery, a double dummy cannula with a 0.5 mm extension beyond the end of the guide cannula with a metal cap, was inserted into the guide cannula. One week after surgery, CGS21680 (0.5 μg/μL) or vehicle (DMSO+PBS) was microinjected into the LS with a drug delivery inner core connected to the microinjection pump. For KW6002 treatment manipulation, KW6002 (istradefylline; 0.5 μg/μL dissolved in 0.5% methylcellulose, synthesized as described previously (67)) or vehicle (methylcellulose + PBS) was microinjected into the LS for a consecutive 3 days after 14 days CRS. The drug (2 μL) was then infused into the LS though the cannula. The injector cannula inner core was left in the LS for an additional 5 min to allow adequate local drug diffusion and minimize spread of the drug along the injection track. Only data with a correct site of injection, confirmed by HE-stain, were used.

Animals stress models

Male mice (8 weeks old) were used in the stress-related experiments. Before starting any stress paradigm, mice with matched age and weight were randomly assigned into the non-stress or stress groups.

Chronic Restraint Stress (CRS)

CRS was performed in 50 mL centrifuge tubes with holes for ventilation. Mice were restrained horizontally in tubes for 3 h in the first 7 days and for 4-5 h in the next 7 days (up to 14 days) (53). Non-stressed mice were left undisturbed in their home cages.

5 days repeated forced swim stress (5d-RFSS)

The mice were subjected to repeat swimming in a transparent cylinder (15 cm diameter, 25 cm height) containing 20 cm of water (22–25℃) for 10 min daily for 5 consecutive days (induction phase). From day 6 on, the mice were kept in the home cage without swimming for 4 weeks, after which a last swim was imposed on day 32 (test phase) (34).

Behavioral Tests

All behavior tests were performed between 10:00 AM and 5:00 AM in a sound attenuation booth and were recorded on videotape for offline analysis with the EthoVision XT system. Between trials, the chamber was cleaned with 70% ethanol. All behavioral experiments were carried out with the experimenter blind to genotype and/or treatment history.

Open field test (OFT)

Animals were individually placed in the center of a chamber (40 x 40 x 40 cm) in a soundproof environment with gentle light and their movement was analyzed during 10 min.

Tail suspension test (TST)

449 The mice tails were wrapped with tape at approximately 1 cm from the end of the tail. The mice were
450 then fixed upside down on a horizontal bar with the nose tip about 30 cm above the ground. Animal
451 behaviors' were recorded for 6 min and the immobility time during the last 4 min was analyzed.

452

453 Elevated O maze

454 The maze was constructed in a circular track 10 cm wide, 105 cm in diameter, and elevated 72 cm
455 from the floor. The maze was divided in four quadrants of equal length with two opposing open
456 quadrants with 1 cm high curbs to prevent falls and two opposing closed quadrants with walls 28 cm
457 in height. A 10 min trial under gentle light conditions was carried out with the animal placed in the
458 center of a closed quadrant to analyze their movement.

459

460 Forced swim test (FST)

461 Animals were individually placed in vertical clear glass cylinder (20 cm in diameter, 30 cm in height)
462 filled with water (21-25℃). Water depth was set to prevent mice from touching the glass bottom with
463 their limbs or tails. The test lasted for 6 min and the immobility time was counted from 2 to 6 min.
464 Mice were regarded as immobile when floating motionless or making only movements that were
465 necessary to hold its head above the water.

466

467 Sucrose preference test (SPT)

468 Mice were single housed and habituated with 1% sucrose and water for 2 days and the bottle positions
469 were counterbalanced every 12 h. On the testing day, mice were water and food-deprived for 12 h
470 and then exposed to pre-weighed identical bottles (one bottle of water and one bottle of 1% sucrose)
471 for 12 h in the dark phase. Sucrose preference was calculated by dividing the consumption of sucrose
472 by the total consumed liquid (water and sucrose).

Western blots

For Western blot analysis, brains were quickly removed from euthanized mice and brain regions (septum, striatum, mPFC and hippocampus) were carefully excised with pincers. Tissues were lysed by sonication in ice-cold RIPA lysis buffer (Beyotime) with complete protease inhibitor cocktail (Beyotime) and phosphatase inhibitors mix (Bimake), incubated on a roller for 30 min at 4˚C and cleared by centrifugation at 14,000 rpm for 15 min. The supernatant was collected and the protein concentration was estimated using Enhanced BCA Protein Assay Kit (Beyotime). Samples were diluted in 5x SDS sample buffer and analyzed by SDS-PAGE. Anti-A_{2A}R (Santa Cruz Biotechnology, 1:200) or anti-actin (Proteintech, 1:3000) antibodies were used to evaluate the relative amount of A_{2A}R.

Immunofluorescence staining

For immunofluorescence staining, 60 min after injecting CGS21680 into LS, mice were anesthetized and perfused with PBS followed by 4% paraformaldehyde (PFA) in PBS (pH 7.4). The brains were quickly removed, post-fixed in 4% PFA overnight, and then dehydrated in 30% sucrose solutions in PBS for 3 days. The brain was sectioned to a thickness of 30 μm using a cryostat (Leica CM1950) and preserved in PBS. Free-floating sections were blocked in blocking solution (0.3% Triton X-100 in PBS and 5% normal donkey serum) for 1 h at room temperature. Sections were then incubated with the primary antibody in antibody solution (5% normal goat serum, 0.3% Triton X-100, 1% bovine serum albumin in PBS) overnight at 4 ^{O}C. Sections were then washed with PBS (3x 10 min) and incubated for 2 h at room temperature with the secondary antibodies and DAPI. Finally, sections were washed with PBS (3x 10 min). According to the anatomical location of each brain area (identified with the 4th edition of Mouse Brain Atlas), nine sections containing LS, LHb and DMH were selected for counting. The following antibodies were used: rabbit anti-c-Fos (EMD Millipore, 1:1000); donkey anti-rabbit 488

(Invitrogen, 1:500). All fluorescent image acquisition was performed with a Leica DM6B microscope and a Zeiss LSM 880 NLO confocal microscope.

For immunofluorescence staining after *in vitro* electrophysiology recording, 300 μm slices were collected and post-fixed in 4% PFA overnight. Free-floating sections were blocked in blocking solution (0.3% Triton X-100 in PBS and 10% normal donkey serum) for 1 h at room temperature and then incubated with rabbit anti-GAD65/67 antibody (Abcam, 1:200) in antibody solution (0.3% Triton X-100 in PBS and 5% normal donkey serum) overnight at 4℃. After washing with PBS, the sections were incubated with secondary antibodies (donkey anti-rabbit 488, Invitrogen, 1:500, or Texas Red Avidin D, Vector Laboratories, 1:500).

RNA extraction and quantitative Real-Time PCR

Total RNAs from mice brains were extracted according to the manual by using Trizol reagent (Invitrogen). Reverse transcription was carried out using PrimeScript™ RT Master Mix (Takara). The reaction mixture was incubated for 10 min at 25°C, followed by 50 min at 37°C, then heat inactivated at 70°C for 15 min. Real-time PCR was performed with StepOne Real-time PCR system by iTaq Universal SYBR Green Supermix (Bio-RAD). Relative LS $A_{2A}R$ expression levels were calculated by comparative CT method. Q-PCR primers used were:

$A_{2A}R$ Forward primer: 5′-CCGAATTCCACTCCGGTACA-3′

$A_{2A}R$ Reverse primer: 5′-CAGTTGTTCCAGCCCAGCAT-3′

Acute slice preparation

AAV2/9-hSyn-DIO-EGFP virus was injected into LS of $A_{2A}R$-Cre mice (aged 8 weeks). Two to three weeks later, $A_{2A}R$-Cre mice were anesthetized with 3% isoflurane, perfused with an oxygenated high sucrose and ice-cold slicing solution (in mM: 234 sucrose, 11 glucose, 26 $NaHCO_3$, 2.5 KCl, 1.25 NaH_2PO_4, 10

521 $MgSO_4$ and 0.5 $CaCl_2$; gassed with 95% O_2/5% CO_2). The brains were quickly removed and placed into
522 the oxygenated and ice-cold high sucrose slicing solution for 2-3 min. Coronal slices (300 µm thick)
523 containing the LS (AP +1.8) were sectioned in ice-cold aCSF (in mM: 126 NaCl, 26 $NaHCO_3$, 10 glucose,
524 2.5 KCl, 1.25 NaH_2PO_4, 2 $MgCl_2$, and 2 $CaCl_2$; pH 7.4, bubbled with 95% O_2/5% CO_2) with a Leica VT1200S
525 vibratome. Before recordings, slices were allowed to recover for at least 1 h in aCSF continuously
526 gassed with 95% O_2/5% CO_2.

527

528 **In vitro Electrophysiology**

529 Patch clamp recordings were made from LS neurons under an upright microscope (Olympus). During
530 recording, LS slices were continuously superfused at 2-3 mL/min with oxygenated aCSF and
531 maintained at 32°C. The patch pipettes were pulled with a pipette puller (PC-100, Narishige) from
532 borosilicate glass (Sutter Instrument) and had a resistance of 5-6 MΩ. Electrophysiological recordings
533 were made using a Multiclamp 700B amplifier. Signals were amplified, filtered at 2 kHz and sampled
534 at 10 kHz using Digidata 1550B. Clampfit 10.6 (Molecular Devices) and Mini Analysis Program
535 (Synaptosoft Inc., NJ) were used to analyze offline electrophysiological data.

536 A cell-attached mode was used to assess the effects of $A_{2A}R$ drugs on the excitability of LS-$A_{2A}R^+$
537 neurons. Glass pipettes were filled with intracellular solution (in mM: 130 K-gluconate, 10 KCl, 10
538 HEPES, 10 EGTA, 2 $MgCl_2$, 2 Na_2ATP, 0.3 Na_3GTP). While approaching the cell, positive pressure was
539 applied to the patch pipette. The seal (10 MΩ –> 5 GΩ) between the recording pipette and the cell
540 membrane was obtained by applying suction to the electrode. Action potential currents were
541 recorded in voltage-clamp mode or alternatively in "search" mode, which maintains an average 0 pA
542 holding current. Resting membrane potential and synaptic potentials were recorded in current-clamp
543 mode as described in the RESULTS.

544 In whole-cell patch clamp recordings, a gigaseal was formed between glass pipette and the cell. In the
545 presence of the glutamate receptor blockers 6,7-dinitroquinoxaline-2,3-dione (DNQX, 20 µM, Tocris)

and DL-2-amino-5-phosphonopentanoic acid (DL-AP_5, 100 µM, Tocris), the IPSCs were recorded in voltage clamp mode (V_{Hold}= -60 mV). For chemogenetic experiments, CGS21680 (30 nM) or KW6002 (100 nM) was added through the aCSF.

In order to investigate the morphology of each recorded cell, biocytin (1%, Thermo Scientific) was added to the intracellular solution, allowing its diffusion into the patched neuron during electrophysiological recordings.

Signal cell Reverse transcription quantitative PCR (RT-qPCR)

Cell cytoplasm was harvested by glass pipettes and expelled into 0.5 mL Eppendorf tube containing 2 µL of 5x PrimeScript RT Master Mix (Takara) and 6 µL RNase Free dH_2O, then mixed well. Intracellular pipette solution and RNase Free dH_20 were used as controls during the reverse transcription. This mixture was incubated for 10 min at 25°C, followed by 50 min at 37°C, then heat inactivated at 70°C for 15 min, using the entire cDNA template reaction (10 µL) in the first round of PCR amplification. Each of the first round of reaction was prepared as follows: GAPDH F1 1 µL, P1 1 µl; VGAT F1 1 µL, P1 1 µL; cDNA 10 µL, mix 10 µL, ddH_2O 26 µL. For the second round of PCR, the nested primers (internal to the first-round pairs) were used. Each of the second round of reaction was prepared as follows: GAPDH F1 1 µL, P2 1 µL; VGAT F1 1 µL, P2 1 µL; cDNA 1 µL, mix 10 µL, ddH_2O 5 µL. The thermal cycling program of the second round was: 94°C for 1 min, 30 cycles of amplification representing three steps of denaturing, annealing and extension (94°C for 30 s; 55°C for 1 min; 72°C for 1 min) and a final extension at 72°C for 7 min. Amplification products were analyzed on a 2% agarose gel and visualized by staining with ethidium bromide.

RT-PCR primers used were:

GAPDH Forward primer: TGGAAAGCTGTGGCGTGAT

GAPDH Reverse primer1: GTTGCTGTTGAAGTCGCAGG 292

GAPDH Reverse primer2: GACGGACACATTGGGGGTAG 151

GAD67 Forward primer: AATACTACCAACCTGCGCCC

GAD67 Reverse primer1: CCCGTTCTTAGCTGGAAGCA 270

GAD67 Reverse primer2: AACAGGTTGGAGAAGTCGGTC 250

Human subjects

Post-mortem tissues were collected at autopsy at the Portuguese National Legal Institute and Forensic Sciences (INML), after official approval (IM004-21/07/2021). Samples were collected from suicide completers with recorded depression, excluding individuals with other psychiatric conditions such as addiction, eating disorders, schizophrenia or phobia and from age-matched-controls deceased upon car or work accidents or natural causes, excluding individuals consuming psychotropic drugs (except alcohol) based on the toxicological screening done during autopsy. The quality control of brain tissue was based on their pH and on their RNA Integrity Number (RIN), as previously described [65] and the manually dissected lateral septum or BA25 were either immediately processed or frozen rapidly in liquid nitrogen and stored at -80ºC until further use.

Membrane-Binding Assays

To evaluate the density of $A_{2A}R$ by radioligand-binding assays, a selective $A_{2A}R$ antagonist [^{3}H] SCH58261 (6 nM; provided by E. Ongini, Schering-Plough, Milan, Italy) was used. Binding was measured at 25 °C for 4 h with 30–100 µg of protein in a final volume of 200 µL solution containing 50 mM Tris–HCl, 10 mM $MgCl_2$, pH 7.4, as previously described [28], with some modifications. A saturation curve was constructed using five different concentrations of [^{3}H]-SCH58261 (0.3, 0.6, 1, 3 and 10 nM). Specific binding was determined by subtraction of the non-specific binding, which was determined in the presence of 2 µM XAC (from Research Biochemical Inc., Sigma-Aldrich). Each

binding assay data point was performed in duplicate. The binding reactions were stopped by rapid vacuum filtration through glass fiber filters (GF/C filters), which were immediately washed with 4 mL ice-cold buffer. Radioactivity in the filters was determined by scintillation counting with an efficiency of 55–60%. The specific binding from saturation experiments was fitted by non-linear regression to a one binding site equation using the GraphPad Inplot software to determine the binding parameters (dissociation constant, K_D, and maximal number of binding sites, B_{max}).

Statistics

In all behavioral, electrophysiological and molecular experiments, mice were randomly grouped and the offline data statistical analysis was performed blindly using SPSS 16.0 or GraphPad Prism 8.0 (GraphPad, San Diego, California). If viral injection or drug delivery was not correctly sited, the data points were excluded from analyses. All data were checked for normality and homogeneity of variance. Student's t-test (unpaired or paired), Mann-Whitney test, and Wilcoxon test were used to compare means between two groups, and two-way analysis of variance followed by Tukey's or Bonferroni *post hoc* tests were used to determine significant differences among multiple groups. Differences were considered significant if $p < 0.05$. All data were presented as mean ± SEM. No statistical methods were used to predetermine sample sizes, but our sample sizes are similar to those generally employed in comparable studies.

Study approval

Written, informed consent was received from all participants. Post-mortem tissues were collected at autopsy at the Portuguese National Legal Institute and Forensic Sciences (INML), after official approval (IM004-21/07/2021). All animal studies were approved by the Institutional Ethics Committee for Animal Use in Research and Education at Wenzhou Medical University, China.

Author Contributions

Conceptualization: W.G., M.W., P.L.; Methodology: W.G., M.W. P.L.; Formal analysis: W.G., M.W., B.S., ZW.L., W.Z., Y.H., T.X., R.C.; Investigation: W.G., M.W., B.S., ZW.L., W.Z., Y.H., T.X. C.C. L.D.; Resources: Y.D., M.Y., ZQ.L., J.Z., X.Z., F.Y.; Writing - Original Draft: W.G., M.W., P.L.; Writing - Review & Editing: W.G., J.C., R.C.; Visualization: M.W., B.S., ZW.L.; Supervision: J.C.; Project administration: W.G.; Funding acquisition: W.G., J.C., P.L., R.C., X.Z.

Acknowledgments

We thank Dr. Jian-jun Zhang (Institute of Psychology of the Chinese Academy of Sciences) and Dr. Chun Hu (South China Normal University) for thoughtful comments for the manuscript. This work was supported by the National Natural Science Foundation of China (Grant No. 31970948, No. 81871035, No.82071378, No.80222014), the Research Fund for International Senior Scientists (Grant No. 82150710558), Zhejiang Provincial Natural Science Foundation (Grant No. LZ19H090001, No.461220086), the Project of State Key Laboratory of Ophthalmology, Optometry and Vision Science, Wenzhou Medical University (J01-20190101), La Caixa Foundation (LCF/PR/HP17/52190001), Centro 2020 (CENTRO-01-0246-FEDER-000010) and FCT (POCI-01-0145-FEDER-03127, UIDB/04539/2020 and IF/01492/2015).

References

1. Organization, W.H., *Depression and Other Common Mental Disorders: Global Health Estimates.* 2017.
2. WHO, *Mental Health Atlas 2017.* Geneva: World Health Organization, 2018.
3. Malhi, G.S. and J.J. Mann, *Depression.* Lancet, 2018. **392**(10161): p. 2299-2312.
4. Rizzi-Wise, C.A. and D.V. Wang, *Putting together pieces of the lateral septum: multifaceted functions and its neural pathways.* eNeuro, 2021. **8**(6).
5. Wirtshafter, H.S. and M.A. Wilson, *Lateral septum as a nexus for mood, motivation, and movement.* Neuroscience and Biobehavioral Reviews, 2021. **126**: p. 544-559.
6. Sheehan, T.P., R.A. Chambers, and D.S. Russell, *Regulation of affect by the lateral septum: Implications for neuropsychiatry.* Brain Res Rev, 2004. **46**(1): p. 71-117.
7. Wang, D., et al., *Regulation of depression-related behaviors by GABAergic neurons in the lateral septum through periaqueductal gray neuronal projections.* J Psychiatr Res, 2021. **137**: p. 202-214.
8. Wang, H., et al., *Takeda G Protein-Coupled Receptor 5 Modulates Depression-like Behaviors via Hippocampal CA3 Pyramidal Neurons Afferent to Dorsolateral Septum.* Biol Psychiatry, 2021. **89**(11): p. 1084-1095.
9. Besnard, A. and F. Leroy, *Top-down regulation of motivated behaviors via lateral septum sub-circuits.* Mol Psychiatry, 2022.
10. Chen, J.F., H.K. Eltzschig, and B.B. Fredholm, *Adenosine receptors as drug targets--what are the challenges?* Nat Rev Drug Discov, 2013. **12**(4): p. 265-86.
11. Borea, P.A., et al., *Pharmacology of Adenosine Receptors: The State of the Art.* Physiol Rev, 2018. **98**(3): p. 1591-1625.

12. Muran Wang, et al., *Genetic tagging of the adenosine A2A receptor reveals its heterogeneous expression in brain regions.* Frontiers in Neuroanatomy, 2020.
13. Fredholm, B.B., et al., *Actions of caffeine in the brain with special reference to factors that contribute to its widespread use.* Pharmacol Rev, 1999. **51**(1): p. 83-133.
14. Lopes, J.P., A. Pliassova, and R.A. Cunha, *The physiological effects of caffeine on synaptic transmission and plasticity in the mouse hippocampus selectively depend on adenosine A1 and A2A receptors.* Biochem Pharmacol, 2019. **166**: p. 313-321.
15. Ding, M., et al., *Association of coffee consumption with total and cause-specific mortality in 3 large prospective cohorts.* Circulation, 2015. **132**(24): p. 2305-15.
16. Grosso, G., et al., *Coffee, tea, caffeine and risk of depression: A systematic review and dose-response meta-analysis of observational studies.* Mol Nutr Food Res, 2016. **60**(1): p. 223-34.
17. Oliveira, S., et al., *Impact of genetic variations in ADORA2A gene on depression and symptoms: a cross-sectional population-based study.* Purinergic Signal, 2019. **15**(1): p. 37-44.
18. Cunha, R.A., *How does adenosine control neuronal dysfunction and neurodegeneration?* J Neurochem, 2016. **139**(6): p. 1019-1055.
19. Moreira-de-Sa, A., et al., *Adenosine A(2A) receptors as biomarkers of brain diseases.* Front Neurosci, 2021. **15**: p. 702581.
20. Duman, R.S. and G.K. Aghajanian, *Synaptic dysfunction in depression: potential therapeutic targets.* Science, 2012. **338**(6103): p. 68-72.
21. Cunha, G.M., et al., *Increased density and synapto-protective effect of adenosine A2A receptors upon sub-chronic restraint stress.* Neuroscience, 2006. **141**(4): p. 1775-81.

22. Kaster, M.P., et al., *Caffeine acts through neuronal adenosine A2A receptors to prevent mood and memory dysfunction triggered by chronic stress.* Proc Natl Acad Sci U S A, 2015. **112**(25): p. 7833-8.
23. El Yacoubi, M., et al., *Adenosine A2A receptor antagonists are potential antidepressants: evidence based on pharmacology and A2A receptor knockout mice.* Br J Pharmacol, 2001. **134**(1): p. 68-77.
24. Batalha, V.L., et al., *Adenosine A(2A) receptor blockade reverts hippocampal stress-induced deficits and restores corticosterone circadian oscillation.* Mol Psychiatry, 2013. **18**(3): p. 320-31.
25. Yamada, K., et al., *Antidepressant activity of the adenosine A2A receptor antagonist, istradefylline (KW-6002) on learned helplessness in rats.* Psychopharmacology, 2014. **231**(14): p. 2839-2849.
26. Padilla, K.M., et al., *Behavioral changes induced through adenosine A2A receptor ligands in a rat depression model induced by olfactory bulbectomy.* Brain Behav, 2018. **8**(5): p. e00952.
27. Muir, J., J. Lopez, and R.C. Bagot, *Wiring the depressed brain: optogenetic and chemogenetic circuit interrogation in animal models of depression.* Neuropsychopharmacology, 2019. **44**(6): p. 1013-1026.
28. Chen, J.F. and R.A. Cunha, *The belated US FDA approval of the adenosine A2A receptor antagonist istradefylline for treatment of Parkinson's disease.* Purinergic Signal, 2020. **16**(2): p. 167-174.
29. Zingg, B., et al., *AAV-Mediated Anterograde Transsynaptic Tagging: Mapping Corticocollicular Input-Defined Neural Pathways for Defense Behaviors.* Neuron, 2017. **93**(1): p. 33-47.

30. Bao, A.M. and D.F. Swaab, *The human hypothalamus in mood disorders: The HPA axis in the center.* IBRO Rep, 2019. **6**: p. 45-53.
31. Hu, H., Y. Cui, and Y. Yang, *Circuits and functions of the lateral habenula in health and in disease.* Nat Rev Neurosci, 2020. **21**(5): p. 277-295.
32. Crema, L.M., et al., *The effect of unpredictable chronic mild stress on depressive-like behavior and on hippocampal A1 and striatal A2A adenosine receptors.* Physiol Behav, 2013. **109**: p. 1-7.
33. Batalha, V.L., et al., *The caffeine-binding adenosine A2A receptor induces age-like HPA-axis dysfunction by targeting glucocorticoid receptor function.* Sci Rep, 2016. **6**: p. 31493.
34. Serchov, T., et al., *Increased signaling via adenosine A1 receptors, sleep deprivation, imipramine, and ketamine inhibit depressive-like behavior via induction of homer1a.* Neuron, 2015. **87**(3): p. 549-62.
35. Rombo, D.M., et al., *Synaptic mechanisms of adenosine A2A receptor-mediated hyperexcitability in the hippocampus.* Hippocampus, 2015. **25**(5): p. 566-80.
36. Martin-Fernandez, M., et al., *Synapse-specific astrocyte gating of amygdala-related behavior.* Nat Neurosci, 2017. **20**(11): p. 1540-8.
37. Kerkhofs, A., et al., *Adenosine A2A receptors control glutamatergic synaptic plasticity in fast spiking interneurons of the prefrontal cortex.* Front Pharmacol, 2018. **9**: p. 133.
38. Shindou, T., et al., *Presynaptic adenosine A2A receptors enhance GABAergic synaptic transmission via a cyclic AMP dependent mechanism in the rat globus pallidus.* Br J Pharmacol, 2002. **136**(2): p. 296-302.

39. Hong, Z.Y., et al., *An adenosine A receptor agonist induces sleep by increasing GABA release in the tuberomammillary nucleus to inhibit histaminergic systems in rats.* J Neurochem, 2005. **92**(6): p. 1542-9.

40. Minic, Z., et al., *Colocalization of A2a but not A1 adenosine receptors with GABA-ergic neurons in cardiopulmonary chemoreflex network in the caudal nucleus of the solitary tract.* Physiol Rep, 2018. **6**(22): p. e13913.

41. Shin, S., et al., *Drd3 Signaling in the Lateral Septum Mediates Early Life Stress-Induced Social Dysfunction.* Neuron, 2018. **97**(1): p. 195-208 e6.

42. Wang, Y., et al., *mGlu2/3 receptors within the ventral part of the lateral septal nuclei modulate stress resilience and vulnerability in mice.* Brain Res, 2022. **1779**.

43. Troyano-Rodriguez, E., C.R. Wirsig-Wiechmann, and M. Ahmad, *Neuroligin-2 Determines Inhibitory Synaptic Transmission in the Lateral Septum to Optimize Stress-Induced Neuronal Activation and Avoidance Behavior.* Biol Psychiatry, 2019. **85**(12): p. 1046-55.

44. Kaster, M.P., A.R. Santos, and A.L. Rodrigues, *Involvement of 5-HT1A receptors in the antidepressant-like effect of adenosine in the mouse forced swimming test.* Brain Res Bull, 2005. **67**(1-2): p. 53-61.

45. Lukasiewicz, S., et al., *Fluorescence studies of homooligomerization of adenosine A2A and serotonin 5-HT1A receptors reveal the specificity of receptor interactions in the plasma membrane.* Pharmacol Rep, 2007. **59**(4): p. 379-92.

46. Zheng, Z., et al., *Hypothalamus-habenula potentiation encodes chronic stress experience and drives depression onset.* Neuron, 2022. **110**(8): p. 1400-15

47. Proulx, C.D., O. Hikosaka, and R. Malinow, *Reward processing by the lateral habenula in normal and depressive behaviors.* Nat Neurosci, 2014. **17**(9): p. 1146-52.

48. Mirrione, M.M., et al., *Increased metabolic activity in the septum and habenula during stress is linked to subsequent expression of learned helplessness behavior.* Front Hum Neurosci, 2014. **8**: p. 29.
49. Li, Y., et al., *Role of the lateral habenula in pain-associated depression.* Front Behav Neurosci, 2017. **11**: p. 31.
50. Li, K., et al., *betaCaMKII in lateral habenula mediates core symptoms of depression.* Science, 2013. **341**(6149): p. 1016-20.
51. Cui, Y., et al., *Astroglial Kir4.1 in the lateral habenula drives neuronal bursts in depression.* Nature, 2018. **554**(7692): p. 323-327.
52. Liu, B., et al., *Excitatory transmission from ventral pallidum to lateral habenula mediates depression.* World J Biol Psychiatry, 2020. **21**(8): p. 627-33.
53. Yang, Y., et al., *Ketamine blocks bursting in the lateral habenula to rapidly relieve depression.* Nature, 2018. **554**(7692): p. 317-22.
54. Sartorius, A., et al., *Remission of major depression under deep brain stimulation of the lateral habenula in a therapy-refractory patient.* Biol Psychiatry, 2010. **67**(2): p. e9-e11.
55. Zhang, C., et al., *Bilateral Habenula deep brain stimulation for treatment-resistant depression: clinical findings and electrophysiological features.* Transl Psychiatry, 2022. **12**(1): p. 52.
56. Svenningsson, P., et al., *Distribution, biochemistry and function of striatal adenosine A2A receptors.* Prog Neurobiol, 1999. **59**(4): p. 355-96.
57. Svenningsson, P., et al., *Distribution of adenosine receptors in the postmortem human brain: an extended autoradiographic study.* Synapse, 1997. **27**(4): p. 322-35.

58. Rosin, D.L., et al., *Immunohistochemical localization of adenosine A2A receptors in the rat central nervous system.* J Comp Neurol, 1998. **401**(2): p. 163-86.
59. Gomez-Castro, F., et al., *Convergence of adenosine and GABA signaling for synapse stabilization during development.* Science, 2021. **374**(6568): p. eabk2055.
60. Viana da Silva, S., et al., *Early synaptic deficits in the APP/PS1 mouse model of Alzheimer's disease involve neuronal adenosine A2A receptors.* Nat Commun, 2016. **7**: p. 11915.
61. Rebola, N., et al., *Long-term effect of convulsive behavior on the density of adenosine A1 and A 2A receptors in the rat cerebral cortex.* Epilepsia, 2005. **46 Suppl 5**: p. 159-65.
62. Crespo, M., D.A. Leon-Navarro, and M. Martin, *Early-life hyperthermic seizures upregulate adenosine A2A receptors in the cortex and promote depressive-like behavior in adult rats.* Epilepsy Behav, 2018. **86**: p. 173-178.
63. He, X.H., et al., *Upregulation of adenosine A2A receptor and downregulation of GLT1 is associated with neuronal cell death in Rasmussen's encephalitis.* Brain Pathol, 2020. **30**(2): p. 246-260.
64. Li, W., et al., *Inactivation of adenosine A(2A) receptors reverses working memory deficits at early stages of Huntington's disease models.* Neurobiol Dis, 2015. **79**: p. 70-80.
65. Rodrigues, M.S., et al., *Brain iron deficiency changes the stoichiometry of adenosine receptor subtypes in cortico-striatal terminals: Implications for Restless Legs Syndrome.* Molecules, 2022. **27**(5): p. p. 1489.
66. Goncalves, N., et al., *Caffeine alleviates progressive motor deficits in a transgenic mouse model of spinocerebellar ataxia.* Ann Neurol, 2017. **81**(3): p. 407-418.

67. Hockemeyer, J., J.C. Burbiel, and C.E. Muller, *Multigram-scale syntheses, stability, and photoreactions of A2A adenosine receptor antagonists with 8-styrylxanthine structure: potential drugs for Parkinson's disease.* J Org Chem, 2004. **69**(10): p. 3308-18.

Figures and Figure Legends

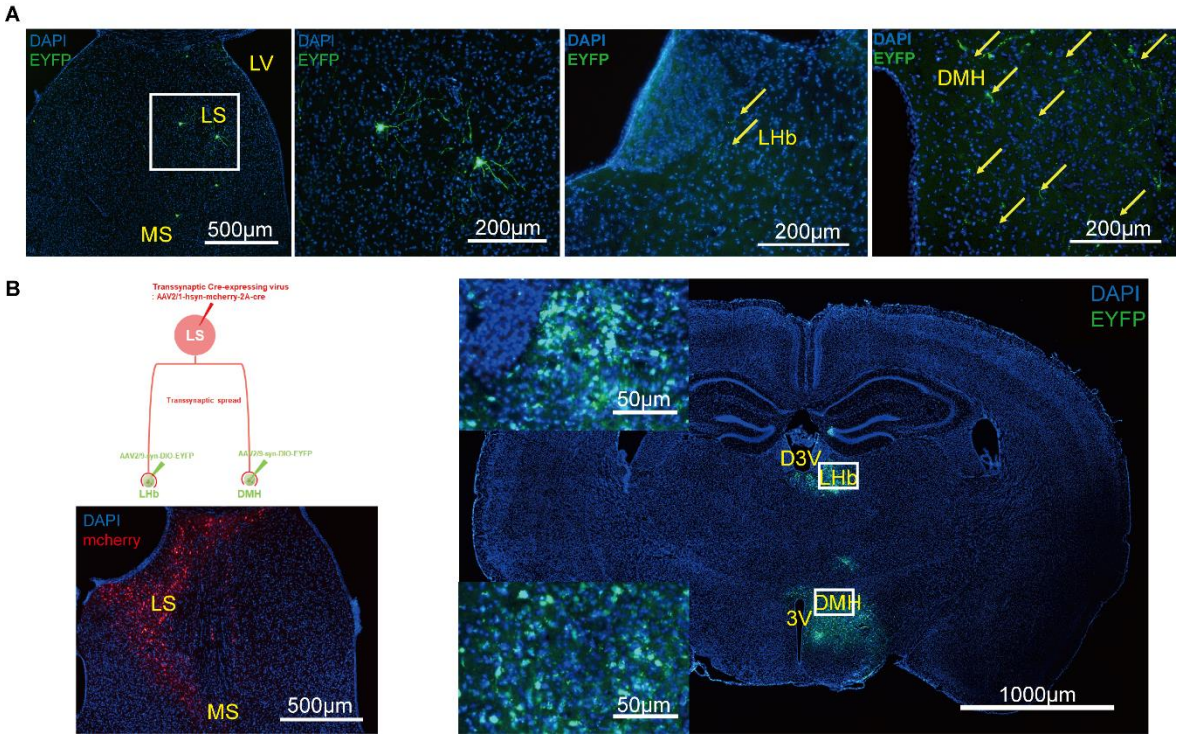

Figure 1. Dorsomedial hypothalamus (DMH) and lateral habenula (LHb) are the main outputs of the lateral septum (LS)

(A) Confocal images of coronal sections showing LS A2AR+ neurons terminals in the DMH and LHb. Three weeks after injecting AAV2/9-syn-DIO-EYFP into the LS of A2AR-Cre mice, GFP-positive projection terminals were found in the DMH and LHb. Scale bar: 500/200 μm. (B) Injecting anterograde trans-synaptic tagging virus AAV2/1-hSyn-mcherry-cre (red) in LS and virus AAV2/9-syn-DIO-EYFP (green) in either LHb or DMH confirmed the direct connectivity from LS to LHb and DMH. Scale bar: 500/1000/50 μm.

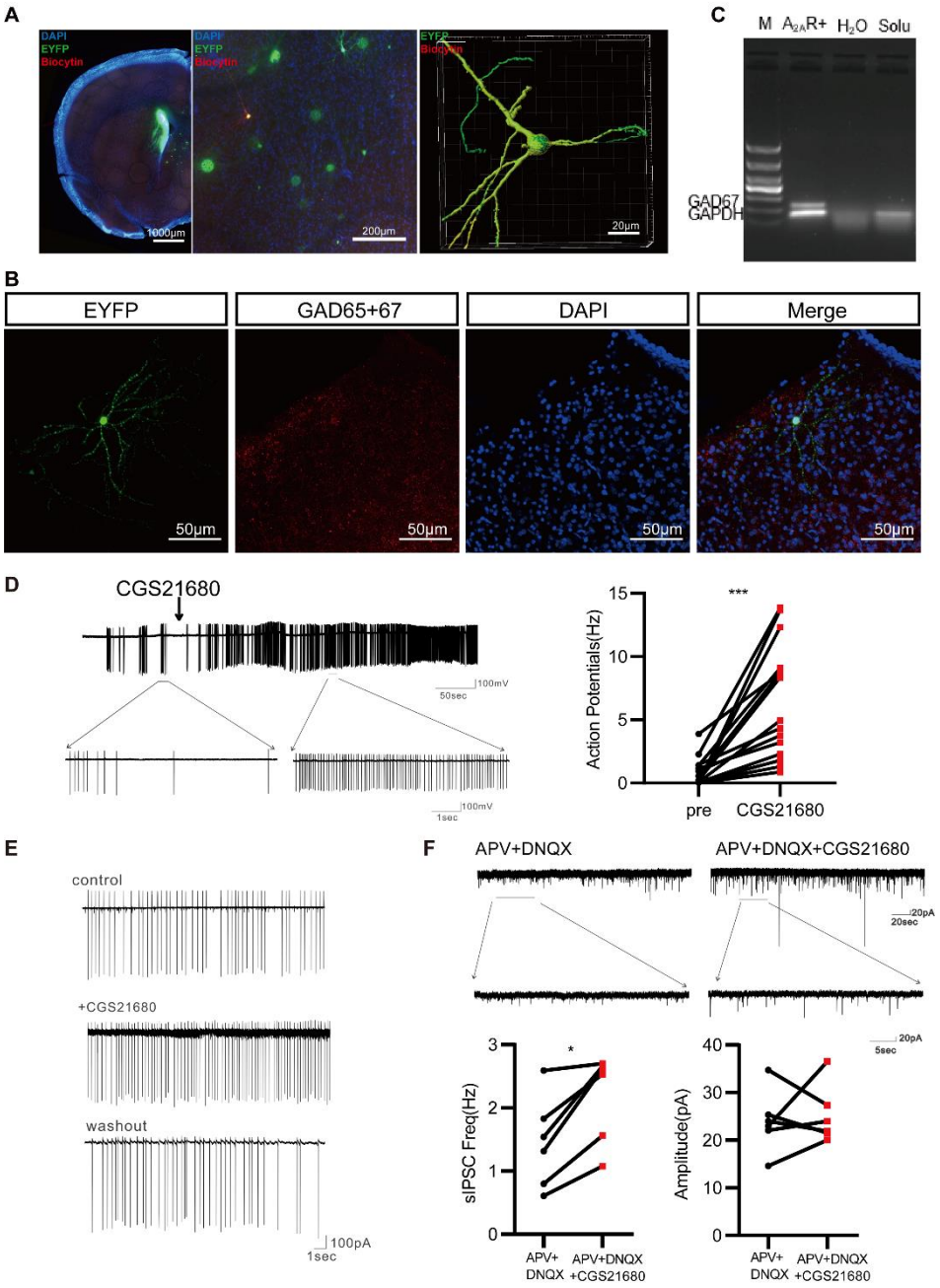

820

821 **Figure 2. Activation of $A_{2A}R$ in the lateral septum (LS) augments spiking frequency of LS-$A_{2A}R^+$**

822 **neurons with suppression of surrounding neurons**

823 (A) Biocytin (red) in the intracellular solution diffused into the cells on brain slices from $A_{2A}R$-Cre mice

824 injected with AAV2/9-hSyn-DIO-EYFP into LS during the in vitro electrophysiological recordings. The

825 recorded $A_{2A}R^+$ neurons (stained yellow) displayed long and numerous branches observed using

826 confocal microscopy combined with 3D surface volume rendering. Scale bar: 1000/200/20 μm. (B)

827 $A_{2A}R^+$ neurons (green) co-immunostained with anti-GAD65/67 antibody (red) in LS. Nuclei stained with

DAPI in blue. Scale bar: 50 µm. (C) Single cell RT-PCR analysis with total mRNA isolated from recorded cells showed that all EYFP-positive cells were GABAergic neurons. (D) Representative trace and statistical graph showing that the activation of $A_{2A}R$ by CGS21680 (30 nM) increased the firing frequency of EYFP-positive neurons (n=16 cells, 8 mice). (E) Representative trace showing that the effect of CGS21680 on EYFP-positive neurons was reversible after washout. (F) Up: Representative voltage-clamp recording showing the alterations of sIPSC (recorded upon blockade of glutamatergic activity 50 µM APV and 20 µM DNQX) in LS non-$A_{2A}R^+$ neurons surrounding $A_{2A}R^+$ neurons before and after the application of CGS21680 (30 nM). Down: Statistical graph showing that CGS21680 increased sIPSCs frequency, without altering their amplitude (n=7 cells, 4 mice). Data are mean ± SEM (Wilcoxon test, *p<0.05, ***p<0.001).

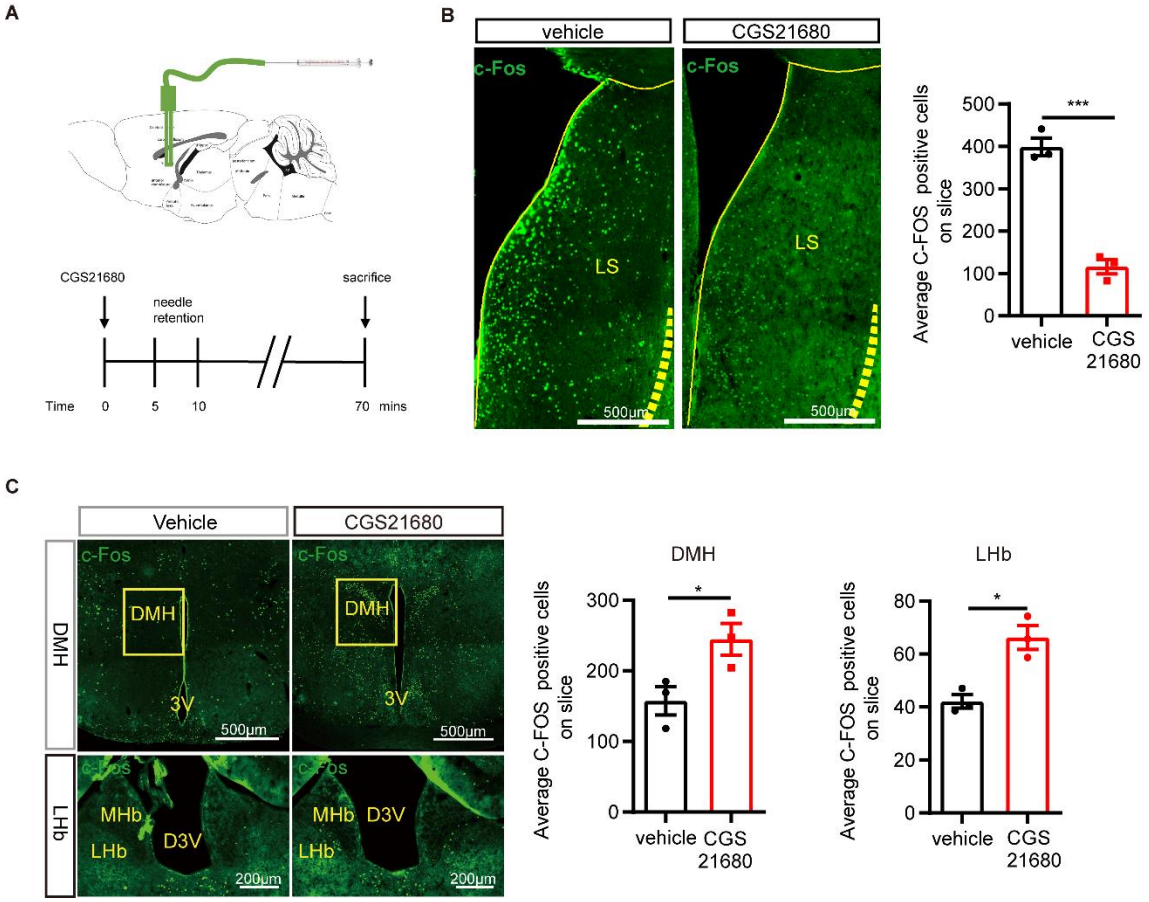

Figure 3. $A_{2A}R$ agonist CGS21680 injection into the lateral septum (LS) suppresses c-Fos expression in the LS and increases c-Fos expression in the LHb and DMH

(A) Schematic protocol for investigating the role of the $A_{2A}R$ agonist CGS21680. (B) Representative immunofluorescence images and average bar graph illustrating the decreased expression of c-Fos in LS (n=3 mice/group, each mice include 9 slices). Scale bar: 500 μm. (C) Representative immunofluorescence images and statistical graphs illustrating the increased expression of c-Fos in DMH and LHb after focal microinjection of the $A_{2A}R$ agonist CGS21680 into LS (n=3 mice/group, each mice include 9 slices). Scale bar: 500/200 μm. Data are mean ± SEM (unpaired t-test, *p<0.05, ***p<0.001).

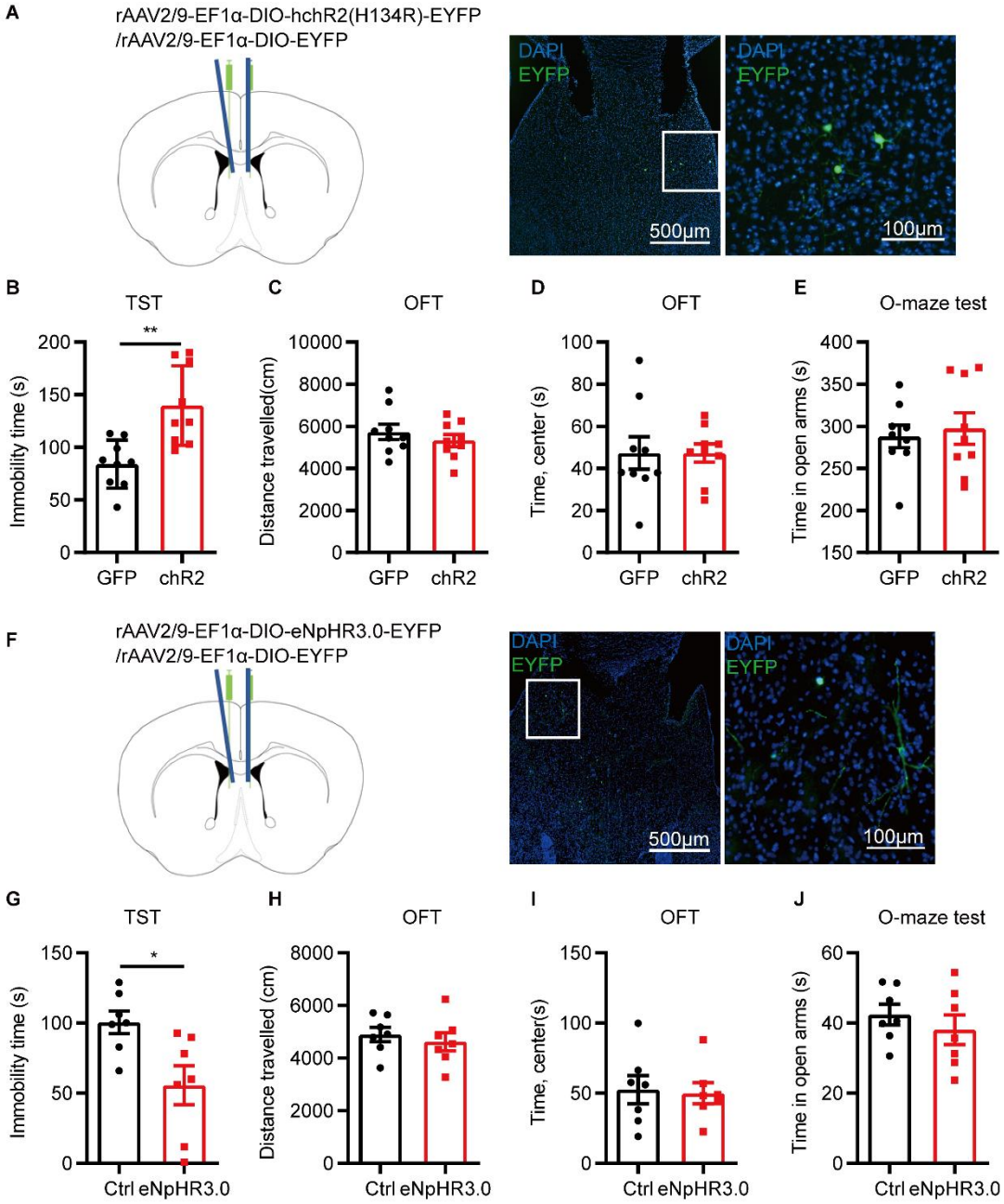

Figure 4. Optogenetic modulation of the activity of A2AR+ neurons in the lateral septum (LS) influences depressive-like phenotype

(A) Left: Schematic illustration of the location of virus injection and optic fibers implantation in $A_{2A}R$-Cre mice. Right: A representative fluorescent image showing the ChR2-positive neurons (green) and the localization of the optic fibers. Nuclei are stained with DAPI in blue. Scale bar:500/100 μm. (B-E) Optogenetic activation of LS-$A_{2A}R^{+}$ neurons increased the immobility time in the tail suspension test (TST) (B) without affecting the total distance travelled (C) or the time in the central area in the open

858 field (OF) test (D) and in the O maze test (E) (n=9 mice/group). (F) Left: Schematic illustration of the
859 location of virus injection and optic fibers implantation in A_{2A}R-Cre mice. Right: A representative
860 fluorescent image shows the eNPHR3.0 positive neurons (green) and the sites of optic fibers. Nuclei
861 stained with DAPI in blue. Scale bar: 500/100 μm. Optogenetic suppression of LS A_{2A}R-positive neurons
862 decrease the immobility time in the tail suspension test (TST) (G), without affecting the total
863 movement distance in the open field (OF) test (H), the time spending in the central area of open field
864 (I), and the duration in the open arm of the O-maze (J) (n=7 mice/group). Data are mean ± SEM
865 (unpaired t test, *p<0.05, **p < 0.01).
866

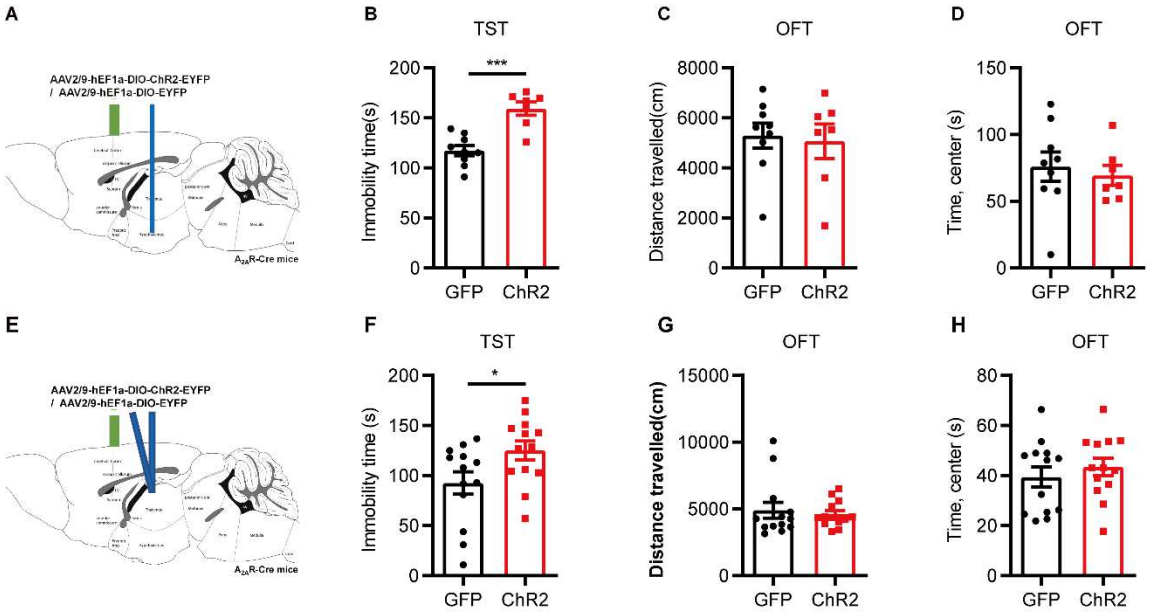

Figure 5. Optogenetic activation of the projection terminals in the dorsomedial hypothalamus (DMH) and lateral habenula (LHb) of A_{2A}R-containing neurons in the lateral septum (LS) reproduced depressive-like behaviors

(A-D) Schematic representation of the optogenetic activation of the LS-A_{2A}R-DMH terminals (A). Optogenetic activation of LS-DMH projection terminals of A_{2A}R-containing neurons increased immobility in the tail suspension test (TST) (B), without altering the total distance travelled and the time spent in the center in the open field (OF) test (C, D) (n=9/7 mice/group). Data are mean ± SEM (unpaired t-test, $^{**}p<0.01$). (E-H) Schematic representation of the optogenetic activation of the LS-A_{2A}R-LHb terminals (E). Optogenetic activation of LS-LHb projection terminals increased immobility in TST (F), without altering the total distance travelled and the time spent in the center in an OF test (G, H) (n=13 mice/group). Data are mean ± SEM (Mann-Whitney test, $^{*}p<0.05$).

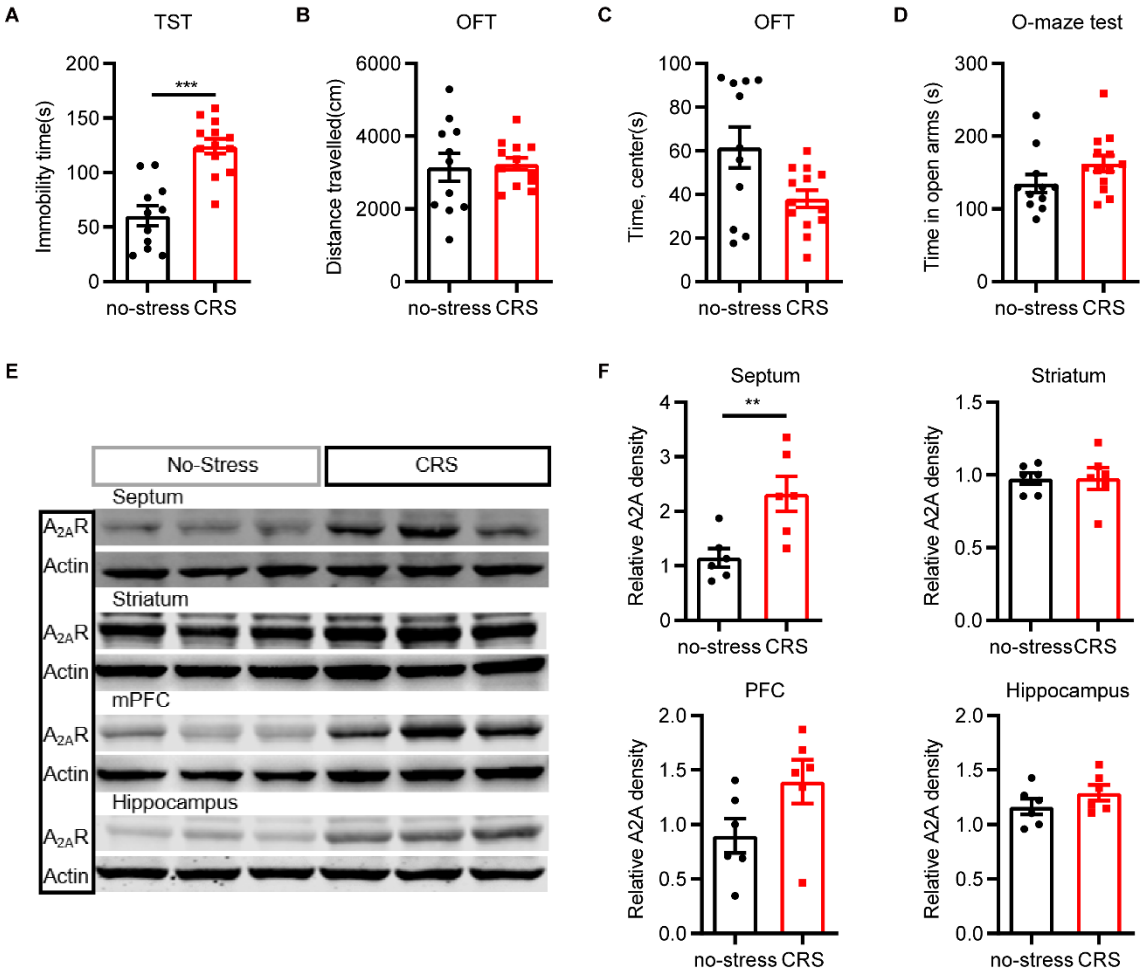

Figure 6. $A_{2A}R$ are selectively upregulated in the lateral septum (LS) in chronic restricted stress (CRS) model

(A-D) Compared with control mice (n=11), CRS mice (n=13) showed an increase in immobility time in a tail suspension test (TST) (A) (unpaired t-test), without changes in the total distance travelled in an open field (OF) test (B) (unpaired t-test). CRS mice spent similar time in the center area of an OF (C) (Mann-Whitney test) and in the open arms of an O-maze test (D) (unpaired t-test). n=11, 13/group, data are mean ± SEM (***p<0.001). (E, F) Representative Western blot and quantification of $A_{2A}R$ protein levels in the septum, prefrontal cortex (PFC), hippocampus, and striatum of CRS and control mice (n=6 /group). CRS mice displayed a selective upregulation of $A_{2A}R$ in the septum without significant changes in the other three brain regions. Data are mean ± SEM (unpaired t-test, **p<0.01).

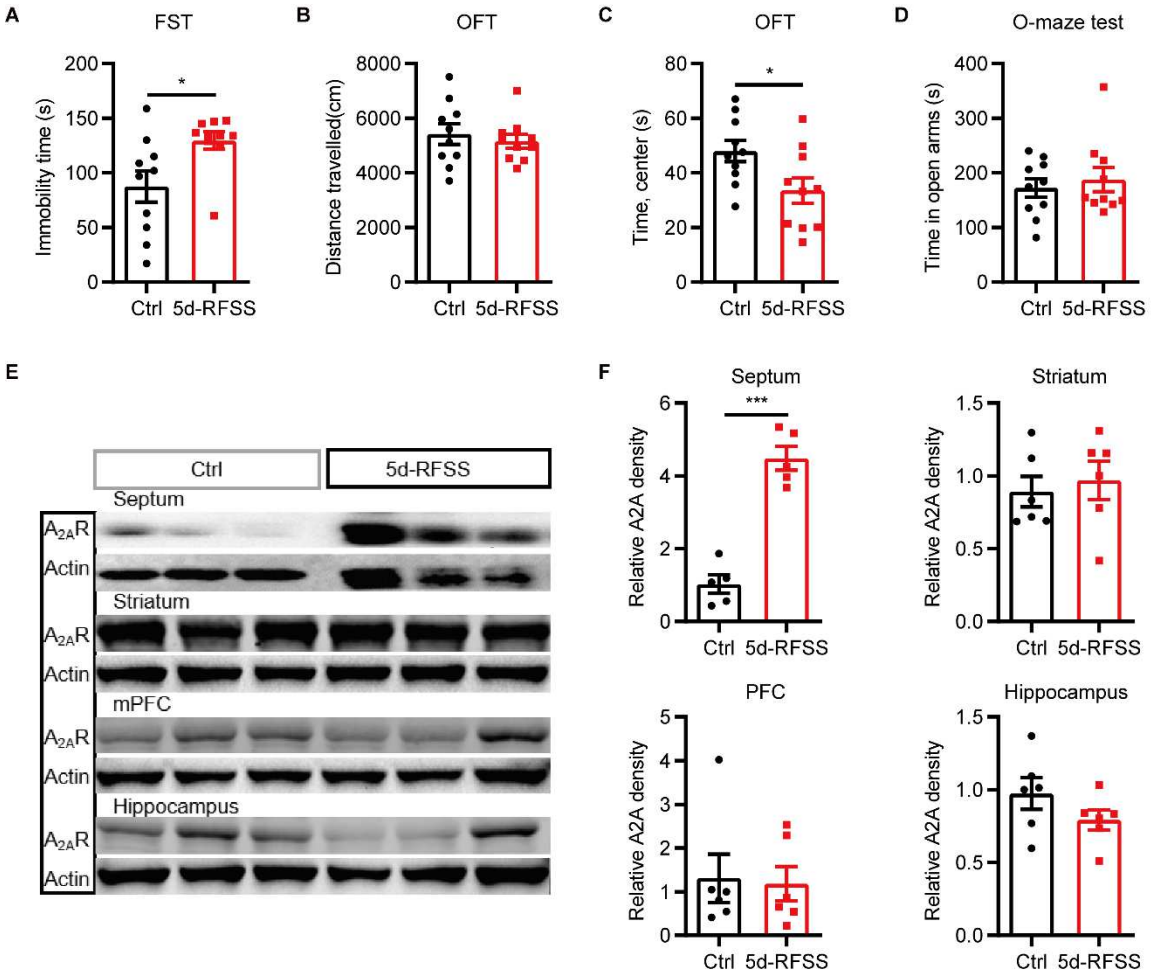

Figure 7. $A_{2A}R$ are selectively upregulated in the lateral septum (LS) in the 5 days repeated forced swim stress (5d-RFSS) model

(A-D) Compared to control mice (n=10), 5d-RFSS mice (n=10) showed increased immobility time in a forced swimming test (FST) (A) (Mann-Whitney test) and reduced time in the central area in an open field (OF) test (B), without change of the total distance travelled in OF (C) (unpaired t-test) and time spent in the open arms in an elevated O-maze test (D) (Mann-Whitney test). (E, F) Representative Western blot and quantification of $A_{2A}R$ protein levels in the septum (unpaired t-test), prefrontal cortex (PFC) (Mann-Whitney test), hippocampus (unpaired t-test) and striatum (Mann-Whitney test) of 5d-RFSS and control mice (n=6/group). 5d-RFSS mice displayed a selective upregulation of $A_{2A}R$ in the septum without significant changes in the other three brain regions. Data are mean ± SEM (unpaired t-test, *p<0.05, ***p<0.001).

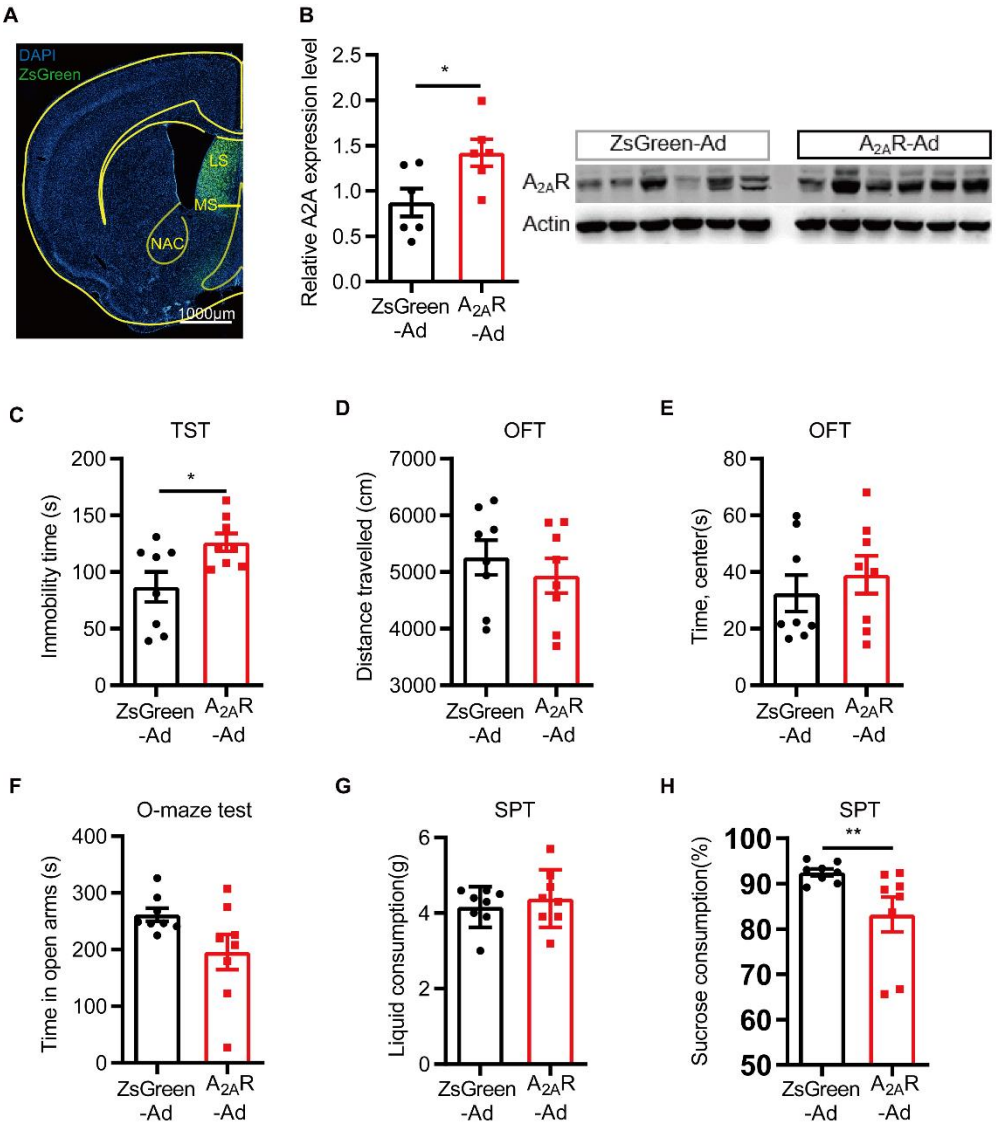

Figure 8. $A_{2A}R$ overexpression in the lateral septum (LS) induces depression-like behaviors

(A) Adenovirus expressing $A_{2A}R$ ($A_{2A}R$-Ad) and ZsGreen (ZsGreen-Ad) in LS. Nuclei are stained with DAPI in blue. Scale bar: 1000 μm. (B) Representative Western blots and quantification of A_{2A} receptor protein levels of mice injected with $A_{2A}R$-Ad and ZsGreen-Ad (unpaired t-test). (C-H) Compared to control mice (n=9), $A_{2A}R$-Ad mice (n=9) displayed increased immobility in the tail suspension test (TST) (C) (unpaired t-test), no change of the total distance travelled (D) (unpaired t-test) or the time in the central area in the open field (OF) test (E) (Mann-Whitney test) and O maze test (F) (unpaired t-test). $A_{2A}R$-Ad mice (n=8) displayed similar total liquid consumption (G) (unpaired t test) but a decreased

914 consumption of sucrose compared with the control group (H) (Mann-Whitney test). Data are mean ±

915 SEM (unpaired t-test, *p<0.05).

916

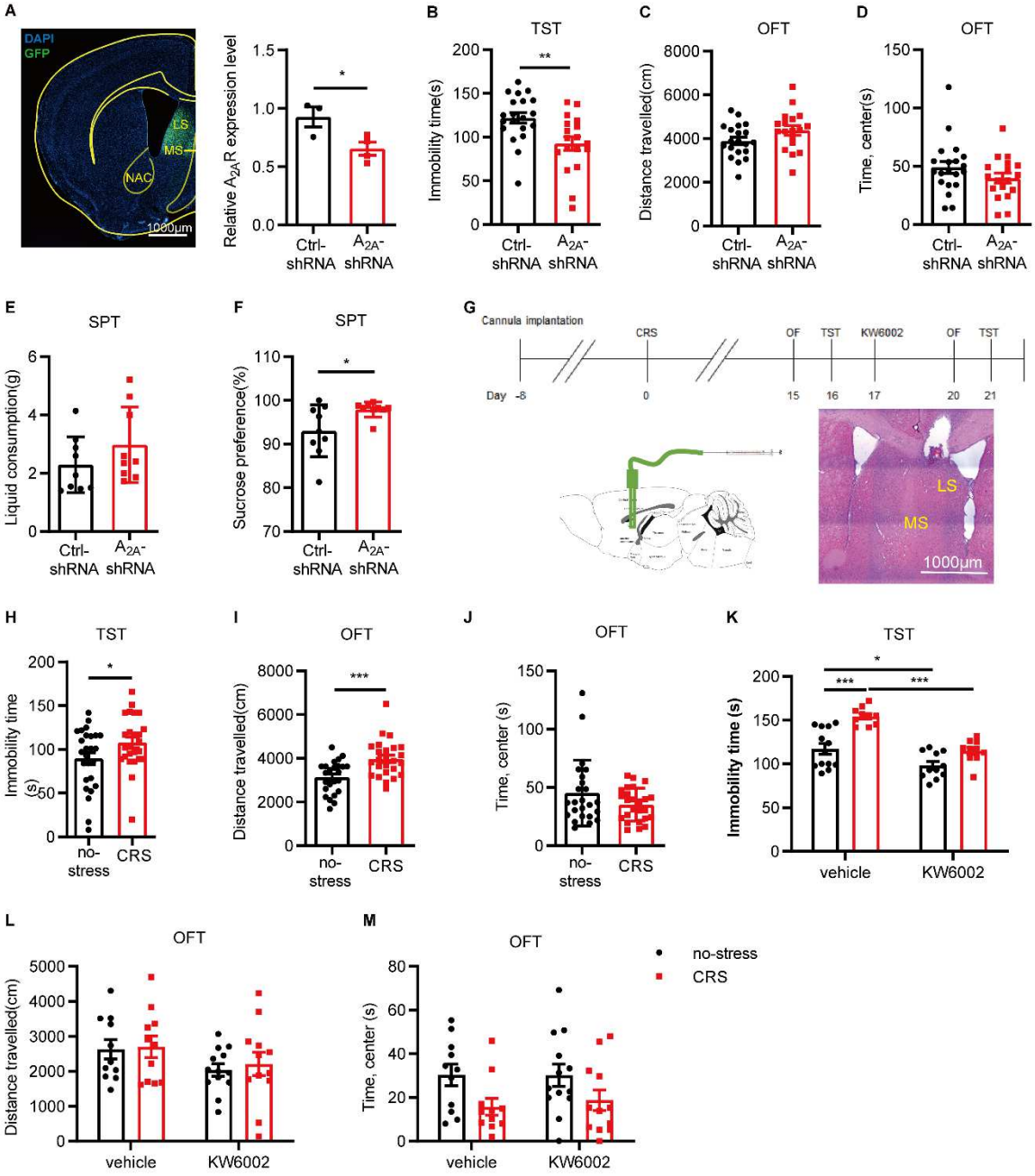

Figure 9. Focal genetic and pharmacological inactivation of $A_{2A}R$ in the lateral septum (LS) affords an anti-depressant-like phenotype

(A) Left: $A_{2A}R$-specific interference virus (AAV9-syn-$A_{2A}R$-shRNA-EGFP) and control virus (AAV9-syn-$A_{2A}R$-shcontrol-EGFP) were injected in LS of C57BL/6J mice. Nuclei are stained with DAPI in blue. Scale bar: 1000 µm. Right: The downregulation of A_{2A} in LS was verified by qPCR (n=3/group) (unpaired t-test). (B) Knockdown of $A_{2A}R$ (n=18-20 mice/group) reduced immobility in the tail suspension test (TST) (unpaired t-test) without affecting basic motor activity (unpaired t-test) and time spent in the central

area (Mann-Whitney test) in the open field (OF) test (C, D). (E, F) LS-$A_{2A}R$ knockdown displayed similar total liquid consumption but increased the consumption of sucrose compared with control mice (n=9 mice/group; Mann-Whitney test). (G) Schematic protocol for investigating the role of the $A_{2A}R$ antagonist KW6002 to reverse the CRS-induced depressive phenotypes. HE staining showing the position of the cannulas. Scale bar: 1000 μm. (H-J) After confirming the depressive-like behaviors in the CRS model by TST (G) and OF test (H, I) (unpaired t-test, Mann-Whitney test, *p<0.05, ***p<0.001), (K-M) injection of KW6002 (0.5 μg/μL, 2 μL) into LS for three consecutive days can reverse the increased immobility in TST caused by CRS (K), but did not affect the performance of mice in OF test (L, M) (n=11-13group; Two-way ANOVA with Bonferroni post hoc test, *p<0.05, ***p<0.001). Data are mean ± SEM.

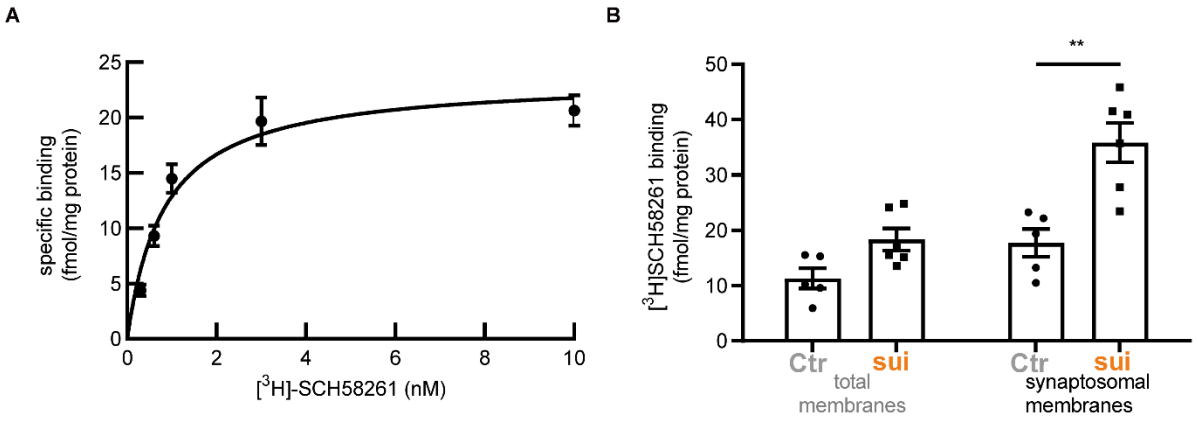

937

938 **Figure 10. $A_{2A}R$ are upregulated in the postmortem lateral septum (LS) of suicide completers**

939 (A) Receptor binding quantification was inferred from the saturation isotherm of [^{3}H]SCH58261

940 binding to membranes of the subgenual area BA25 of 5 controls. (B) Brain tissues from 6 suicide

941 completers with previous record of depressive conditions and 5 age-matched psychiatrically healthy

942 control subjects were collected and processed to prepare total membranes and synaptosomal

943 membranes used for quantitative radioligand receptor binding analysis with 2 nM of the $A_{2A}R$

944 antagonist - [^{3}H]SCH58261. The binding density in synaptosomal membranes (unpaired t-test,

945 **p<0.01), but not the total membranes (Mann-Whitney test, p=0.0519), increased in suicide

946 completers compared to control subjects. Data are mean ± SEM.

947